Cell

Short article

# Molecular impact of antisense oligonucleotide therapy in *C9orf72*-associated ALS

## Graphical abstract

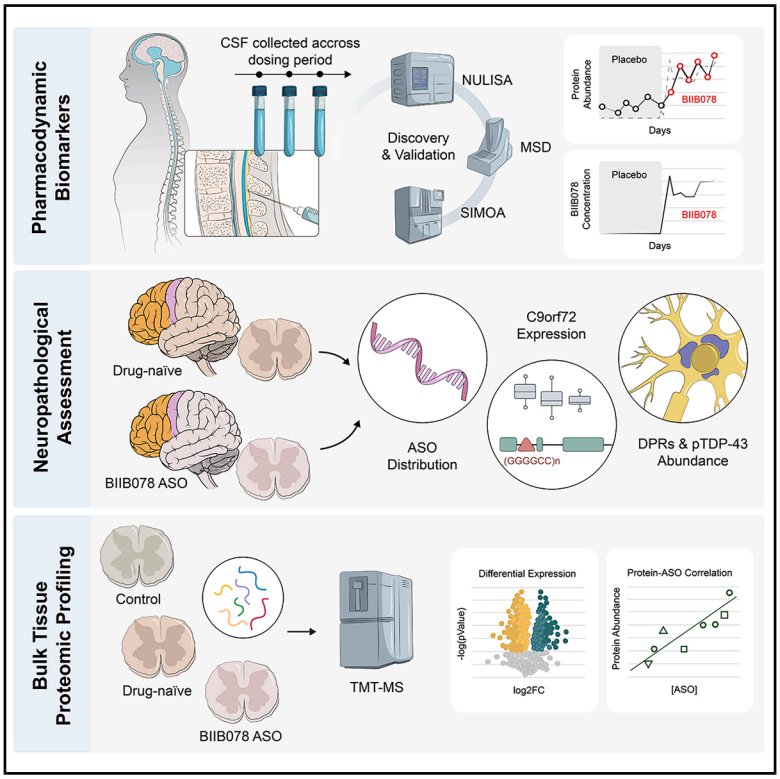


## Highlights

- Intrathecally delivered BIIB078 ASO results in broad and sustained CNS penetration
- *C9orf72*-associated pathologies persist in BIIB078 ASO-treated patient tissues
- CCL26 is a pharmacodynamic biomarker of BIIB078 ASO treatment
- Overall proteomic impact of BIIB078 ASO is minimal, apart from an increase in RNase T2

## Authors

Zachary T. McEachin, Mingee Chung, Sabrina A. Stratton, ..., Tania F. Gendron, Nicholas T. Seyfried, Jonathan D. Glass

## Correspondence

zmceach@emory.edu (Z.T.M.), nseyfri@emory.edu (N.T.S.), jglas03@emory.edu (J.D.G.)

## In brief

This study provides an in-depth examination of the effects of BIIB078 antisense oligonucleotide therapy (ASO) in ALS patients with *C9orf72* mutations. Although the drug reached the brain and spinal cord, it did not significantly reduce key pathological features of the disease. This study emphasizes the need for new and reliable biomarkers for ASO therapy, with broad implications for treatment of other diseases.

McEachin et al., 2025, Cell *188*, 1–12
November 13, 2025 
https://doi.org/10.1016/j.cell.2025.07.045

CellPress

Please cite this article in press as: McEachin et al., Molecular impact of antisense oligonucleotide therapy in *C9orf72*-associated ALS, Cell (2025), https://doi.org/10.1016/j.cell.2025.07.045

Cell

CellPress
OPEN ACCESS

Short article

# Molecular impact of antisense oligonucleotide therapy in *C9orf72*-associated ALS

Zachary T. McEachin,[1,2,3,4,12,*] Mingee Chung,[1,2,3] Sabrina A. Stratton,[1,2,3] Changhee Han,[1,3] Woo Jae Kim,[1,3] Udit Sheth,[5,6] Eleanor V. Thomas,[4,7] Ethan Issenberg,[1,3] Tanvi Kamra,[1,3] Paola Merino,[4,8] Yona Levites,[4,8] Nisha Raj,[1,2,3] Eric B. Dammer,[4,9] Duc M. Duong,[4,9] Lingyan Ping,[4,9] Anantharaman Shantaraman,[4,9] Adam N. Trautwig,[4,9] Joshna Gadhavi,[4,9] Ezana Assefa,[4,7] Marla Gearing,[4,7,10] Kaylor M. Kelly,[4,10] Shanu F. Roemer,[6] Michael DeTure,[6] Seneshaw Asress,[4,7] Thomas Kukar,[4,7,8] Christina Fournier,[7] Dennis W. Dickson,[5,6] Leonard Petrucelli,[5,6] Todd E. Golde,[4,7,8] Björn Oskarsson,[11] Tania F. Gendron,[5,6] Nicholas T. Seyfried,[4,7,9,*] and Jonathan D. Glass[4,7,10,*]

[1]Department of Human Genetics, Emory University, Atlanta, GA 30322, USA
[2]Department of Cell Biology, Emory University, Atlanta, GA 30322, USA
[3]Laboratory for Translational Cell Biology, Emory University, Atlanta, GA 30322, USA
[4]Goizueta Brain Health Institute Center for Neurodegenerative Diseases, Emory University, Atlanta, GA 30322, USA
[5]Mayo Clinic Graduate School of Biomedical Sciences, Mayo Clinic, Jacksonville, FL 32224, USA
[6]Department of Neuroscience, Mayo Clinic, Jacksonville, FL 32224, USA
[7]Department of Neurology, Emory University, Atlanta, GA 30322, USA
[8]Department of Pharmacology & Chemical Biology, Emory University, Atlanta, GA 30322, USA
[9]Department of Biochemistry, Emory University, Atlanta, GA 30322, USA
[10]Department of Pathology, Emory University, Atlanta, GA 30322, USA
[11]Department of Neurology, Mayo Clinic, Jacksonville, FL 32224, USA
[12]Lead Contact
*Correspondence: zmceach@emory.edu (Z.T.M.), nseyfri@emory.edu (N.T.S.), jglas03@emory.edu (J.D.G.)
https://doi.org/10.1016/j.cell.2025.07.045

## SUMMARY

*C9orf72*-associated amyotrophic lateral sclerosis (c9ALS) is caused by an intronic $G_4C_2$ repeat expansion that leads to toxic RNA transcripts and dipeptide repeat proteins (DPRs). A clinical trial using the antisense oligonucleotide (ASO) BIIB078 to target these transcripts was discontinued after failing to provide clinical benefit. Here, we determine the extent of target engagement in the central nervous system (CNS) and elucidate pharmacodynamic cerebrospinal fluid (CSF) biomarkers following treatment. CSF from BIIB078-treated cases showed reduced DPRs and sustained increases in inflammatory biomarkers, including C-C motif chemokine ligand 26 (CCL26). BIIB078 was widely distributed in postmortem CNS tissue; however, DPRs and phosphorylated TDP-43 remained abundant. Proteomic signatures in c9ALS spinal cord were not altered with treatment, although a distinct increase in RNase T2 abundance that correlated with BIIB078 concentration was observed. Thus, despite widespread distribution, BIIB078 did not significantly impact key CNS pathologies, emphasizing the need to identify pharmacodynamic biomarkers that reflect disease-relevant neuropathological changes in response to ASO therapies.

## INTRODUCTION

Amyotrophic lateral sclerosis (ALS) is a progressive neurodegenerative disease characterized by the loss of motor neurons in the motor cortex and spinal cord.[1] The most common genetic cause of ALS and frontotemporal dementia (FTD) is an expanded $G_4C_2$ repeat in the first intron of the gene *C9orf72*.[2,3] The mechanism(s) by which the $G_4C_2$ repeat expansion promotes neurodegeneration remain unknown; however, several lines of evidence implicate toxic gain of function resulting from the bidirectional transcription and translation of expanded repeats.[4] Sense ($G_4C_2$) or antisense ($C_4G_2$) repeat RNAs can sequester RNA-binding proteins (RBPs), disrupting their function.[5–9] Translation of repeat-containing transcripts produces dipeptide repeat proteins (DPRs)[10–12] that have been shown to be toxic through myriad mechanisms.[13–19] Motivated by preclinical and clinical successes in other diseases,[20] antisense oligonucleotides (ASOs) have emerged as a leading therapeutic strategy in *C9orf72*-associated ALS (c9ALS).[7,8,21–27]

BIIB078 (tadnersen) is a mixed-backbone, 4-8-6 "gapmer" ASO composed of a central unmodified DNA gap and flanking 2′-O-methoxyethyl (MOE)-modified RNA wings (GSRS UNII: OSO6W71NMN) designed to target an 18-bp sequence in

Please cite this article in press as: McEachin et al., Molecular impact of antisense oligonucleotide therapy in *C9orf72*-associated ALS, Cell (2025), https://doi.org/10.1016/j.cell.2025.07.045



the first intron of *C9orf72* and to degrade $G_4C_2$ repeat-containing transcripts via RNase-H cleavage. Preclinical studies showed that *C9orf72*-targeting ASOs silenced expression of $G_4C_2$ repeat-containing transcripts and reduced DPR toxicity.[7–9,23–25] A seminal preclinical study demonstrated that a single intracerebroventricular (ICV) injection of a similar ASO delivered to transgenic c9BAC mice silenced expression of $G_4C_2$ repeat transcripts and resulted in a sustained reduction of DPR burden.[25] These studies supported the clinical trial of intrathecal BIIB078 in c9ALS (NCT03626012; NCT04288856). Although clinical results showed reduced cerebrospinal fluid (CSF) poly(GP) and poly(GA) DPR proteins, BIIB078 did not improve clinical outcomes.[28] Here, we conducted molecular and neuropathological analyses of BIIB078-treated c9ALS cases to address key questions: (1) did BIIB078 distribute broadly in the central nervous system (CNS); (2) did it reduce $G_4C_2$ transcripts in CNS parenchyma; (3) did it alter c9ALS pathology; (4) did it trigger an immune response; and (5) did it result in proteomic changes in spinal cord tissue?

## RESULTS

### Fluid biomarkers are variable in c9ALS ASO-treated patients

This study includes eight c9ALS patients treated with BIIB078: four with matched CSF and postmortem tissue, two with postmortem tissue only, and two with CSF only. Drug-naive c9ALS ($n$ = 31) and non-ALS cases ($n$ = 32) were included as controls. Dosing for treated cases and clinical, demographic, and neuropathological data for all cases are summarized in Table S1. In six treated cases with longitudinal CSF sampling, we measured soluble poly(GP), a pharmacodynamic biomarker of target engagement,[24,29,30] and neurofilament light chain (NfL), a prognostic biomarker of ALS[31] and a potential therapeutic response biomarker.[32] Poly(GP) abundance decreased in five of six cases (avg. = −37.2%), with substantial variability across time points (Figures 1A, S1A, and S1B). One case, case #6, exhibited a robust, monotonic reduction in poly(GP) abundance (−77.4%). Near-contemporaneously recorded measurements of neurological function using the ALS Functional Rating Scale-Revised (ALSFRS-R) showed a decline in scores during BIIB078 treatment (Figures 1A, S1A, and S1C). NfL abundance measured before the first and at the last BIIB078 dose also varied across cases: four cases showed increases in NfL, while two showed decreases (Figure S1D).

### BIIB078 concentrations in the CSF do not correlate with poly(GP) abundance

Adapting a plate-based oligonucleotide electrochemiluminescent (POE) immunoassay[33] (Figures S2A–S2D), we assessed BIIB078 concentration in CSF. BIIB078 was detectable at all time points following the initial dose (Figures 1B and S2E). All cases showed a salient spike in CSF BIIB078 concentration after the first two loading doses, administered ∼2 weeks apart, followed by a decline prior to administration of the first maintenance dose (∼1-month interval). Through subsequent maintenance doses, BIIB078 concentrations varied across cases and time points (Figures 1B and S2E). In case #5, BIIB078 remained detectable at 78 and 119 days after the last 10-mg dose but was undetectable at day 429 (Figure S2E). Case #6 (60-mg cohort) uniquely showed a gradual increase in BIIB078 concentration across maintenance doses (Figure 1B). Poly(GP) abundance and BIIB078 concentration in CSF did not correlate in four cases; however, cases #5 and #6 showed a moderate and strong correlation between poly(GP) and BIIB078, respectively (Figures 1C and S2F).

### BIIB078 induces immune-related protein abundance changes

We used the highly sensitive nucleic acid linked immunosandwich assay (NULISA)[34] to profile 79 CSF samples across 6 BIIB078-treated cases (Figure 1D; Table S2). Comparing protein abundances between the first and last doses, we identified increases in pro-inflammatory cytokines or cytokine receptors including tumor necrosis factor (TNF) receptor superfamily member 11b (TNFRSF11B), colony stimulating factor 2 receptor subunit beta (CSFR2B), growth differentiation factor 15 (GDF15), and C-C motif chemokine ligand 26 (CCL26) (Figures 1E and 1F). CCL26 exhibited the most robust and consistent increase in abundance across all cases and time points (Figures 1G and S3A), which was confirmed using an independent immunoassay (Figures 1H, S3B, and S3C). Importantly, CCL26 abundance remained stable during placebo dosing (cf. case #6 and case #8), indicating this was not a response to repeated lumbar punctures or excipient. CCL26 abundance increased following the loading phase, and it remained elevated during maintenance dosing, even when measurable BIIB078 concentration in the CSF declined (e.g., case #8) (Figures 1G, 1H, S3A, and S3B). The NULISA CNS panel also measured NfL, which remained stable throughout dosing (Table S2).

### BIIB078 distributes broadly throughout the CNS parenchyma

Immunohistochemical (IHC) analysis using a polyclonal antibody showed positive staining in the spinal cord, which was more intense and widely distributed in cases with shorter intervals between the last BIIB078 dose and autopsy (Figure 2A).

An orthogonal *in situ* hybridization (ISH) approach using a custom miRNAscope (ACDBio) probe (Figure S4) was more robust than IHC and revealed that BIIB078 was present in the spinal cords of all cases (Figure 2A). Signal intensity was reduced as the interval between the last dose and autopsy increased. BIIB078 was observed in white matter tracts of the dorsal, ventral, and lateral columns as well as in the gray matter of dorsal and ventral horns. Internalization of BIIB078 was detected in both the cytoplasm and nucleus of all cell types in the spinal cord, including motor neurons. Using the ISH probe, BIIB078 was observed throughout subarachnoid brain regions—including the motor, frontal, and cerebellar cortices (Figures 2B–2D; Data S1A–S1C)—as well as periventricular regions of the hippocampus, basal ganglia, and medulla (Figures 2E–2G; Data S1D–S1F). In the motor and frontal cortices, BIIB078 was strongly localized to the

Please cite this article in press as: McEachin et al., Molecular impact of antisense oligonucleotide therapy in *C9orf72*-associated ALS, Cell (2025), https://doi.org/10.1016/j.cell.2025.07.045



CellPress
OPEN ACCESS

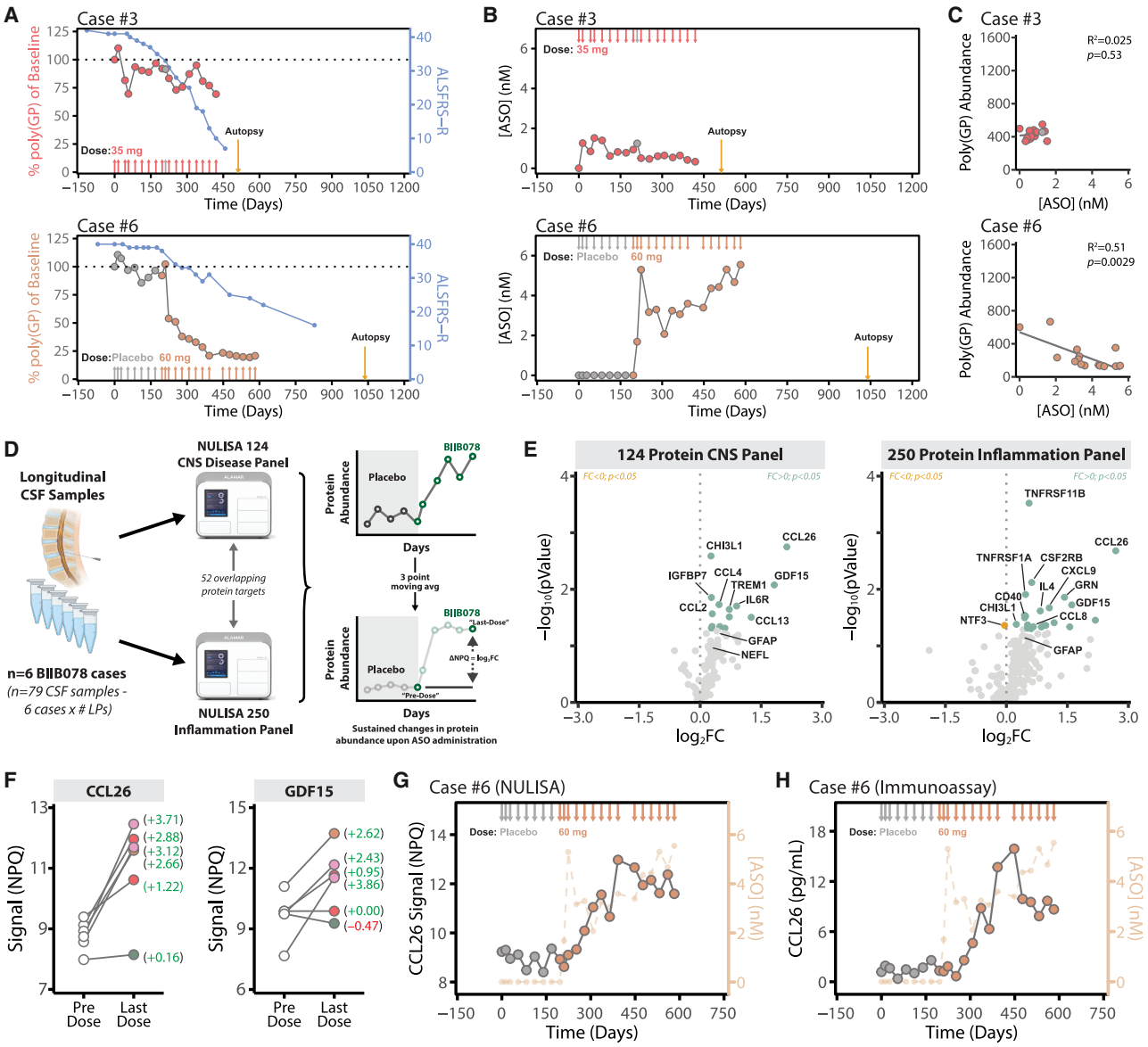


**Figure 1. Assessment and discovery of pharmacodynamic biomarkers in CSF following BIIB078 treatment in c9ALS patients**

(A) Timeline of BIIB078 dosing, CSF poly(GP) abundance, and ALSFRS-R scores. CSF was collected prior to dosing at each time point. Left axis shows relative CSF poly(GP) abundance normalized to a baseline (100%, dotted line); right axis shows ALSFRS-R scores recorded near-contemporaneously.

(B) Timeline of BIIB078 dosing and corresponding CSF BIIB078 concentration. CSF was collected prior to dosing at each time point.

(C) Correlation between CSF BIIB078 concentration and poly(GP) abundance (Pearson correlation).

(D) Schematic of CSF NULISA workflow. 79 CSF samples across 6 different BIIB078 cases were analyzed using the NULISA CNS and inflammation panel. A three-point moving average was applied to smooth pre-dose and last dose values prior to calculating $\log_2$ fold changes ($\log_2$FCs) (ΔNPQ) for volcano plots in (E). LP, lumbar puncture.

(E) Volcano plots showing the $\log_2$ fold changes ($\log_2$FCs) (ΔNPQ, *x* axis) against the t test-derived $-\log_{10}$ statistical *p* value (*y* axis) for protein abundance between smoothed pre-dose and last-dose samples. NULISA protein quantification (NPQ) units are $\log_2$ transformed units.

(F) Slope plots demonstrating changes in raw NPQ units between CSF collected at last dose and immediately preceding initial dose ("pre-dose") for each case. Several proteins including CCL26 (eotaxin-3) and GDF15 showed consistent increases in CSF abundance upon ASO dosing. Numbers in parentheses represent ΔNPQ ($\log_2$FC).

(G) Time course of CCL26 abundance measured by NULISA across dosing intervals. Left axis: NPQ units; right axis: BIIB078 concentration (dotted line).

(H) Validation of CCL26 abundance changes using an orthogonal Mesoscale Discovery (MSD) CCL26 immunoassay.

See Figures S1, S2, and S3.

Please cite this article in press as: McEachin et al., Molecular impact of antisense oligonucleotide therapy in *C9orf72*-associated ALS, Cell (2025), https://doi.org/10.1016/j.cell.2025.07.045



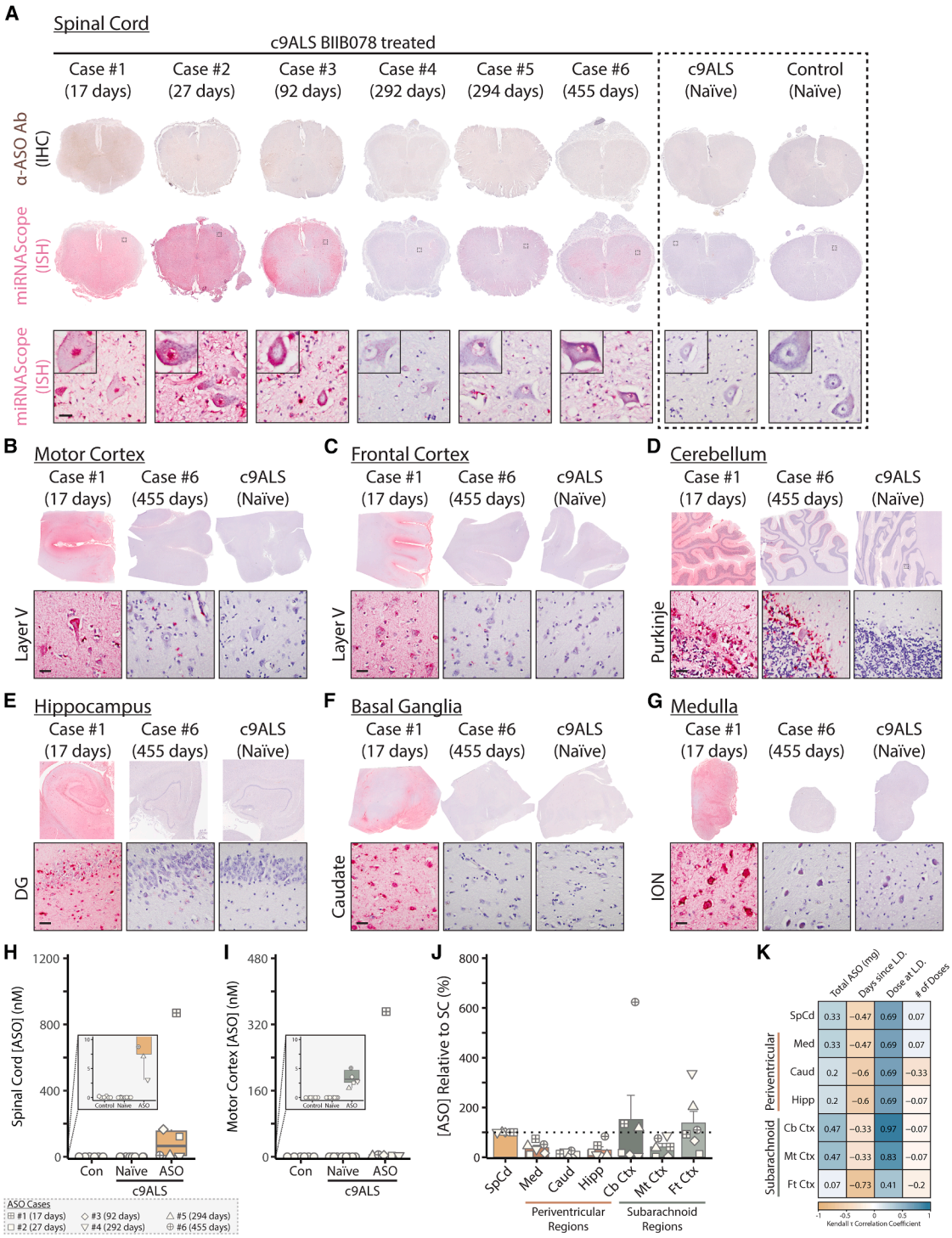


**Figure 2. BIIB078 is broadly distributed throughout the CNS**

(A) Detection of BIIB078 in the spinal cord using anti-ASO IHC staining and miRNAscope *in situ* hybridization (ISH) in control, drug-naive c9ALS (Naive), and BIIB078-treated cases (ASO). BIIB078 signal is present in ventral horn neurons. Numbers in parentheses indicate days between last BIIB078 dose and autopsy. Scale bar, 30 μm.

(B–G) Macro and high magnification images showing BIIB078 distribution by ISH in subarachnoid regions (motor cortex, frontal cortex, cerebellar cortex) and periventricular regions (hippocampus, basal ganglia, medulla). Scale bar, 30 μm.

*(legend continued on next page)*

Please cite this article in press as: McEachin et al., Molecular impact of antisense oligonucleotide therapy in *C9orf72*-associated ALS, Cell (2025), https://doi.org/10.1016/j.cell.2025.07.045



arachnoid and pial linings along sulco-gyral patterns but also penetrated both superficial and deep cortical laminae including the internal pyramidal (layer 5) and multiform (layer 6) layers (Figures 2B and 2C). In cases with a short last dose-to-autopsy interval (e.g., case #1; 17 days), BIIB078 was detectable in neurons, glia, and neuropil. In cases with longer intervals (e.g., case #6; 455 days), BIIB078 was less abundant throughout cortical layers but was observed in cells surrounding Virchow-Robin spaces and the Purkinje layer of the cerebellum. In periventricular regions, BIIB078 signal was observed in regions abutting the respective ventricular space (Figures 2E–2G).

BIIB078 was detected by POE assay in all brain regions examined including spinal cord and motor cortex (Figures 2H, 2I, and S5). To assess relative distribution, BIIB078 concentrations in brain regions were normalized to spinal cord concentrations within each case, which revealed reduced BIIB078 in the periventricular regions and marked variation in subarachnoid regions (Figure 2J). BIIB078 concentration was positively correlated with the dose administered (mg) at last visit and negatively correlated with the interval between the final dose and autopsy (Figure 2K).

## *C9orf72* transcripts are moderately reduced in BIIB078-treated cases

*C9orf72* produces three major transcript variants: V1 (NM_14005.6) and V3 (NM_001256054.2) from exon 1a (with $G_4C_2$ repeats in intron 1) and V2 (NM_018325.5) from exon 1b. BIIB078 was designed to target repeat-containing transcripts, V1 and V3. Quantitative PCR (qPCR) in spinal cord showed no differences in total *C9orf72* transcript levels among controls, drug-naive, and BIIB078-treated cases, although c9ALS cases trended lower (Figure 3A). V3 expression was reduced in treated vs. controls; V1 was unchanged. The lowest V1/V3 levels were observed in cases with a high BIIB078 concentration and short last dose to autopsy interval. In the motor cortex, effects were overall less pronounced (Figure S6A).

To assess intronic $G_4C_2$-containing RNA transcript abundance, we used a custom NanoString probe designed to recognize intron 1 upstream of the $G_4C_2$ repeat. In BIIB078-treated cases, there was a trend toward lower intronic $G_4C_2$-containing transcripts, compared with drug-naive c9ALS (Figure S6B), with the lowest expression in those cases treated with the highest doses. We also assessed the $C_4G_2$-containing antisense transcript using a custom NanoString probe and found the expected increase in antisense transcripts in c9ALS, compared with controls, but found no difference between drug-naive and BIIB078-treated cases (Figure S6B). Using tandem mass tag mass spectrometry (TMT-MS) there was no difference in C9orf72 protein abundance in the spinal cord comparing drug-naive and BIIB078 cases (Figure 3B).

## DPR and TDP-43 pathology persist in BIIB078-treated patients

Immunostaining for poly(GP) and poly(GA) showed inclusions in the spinal cord, motor cortex, and frontal cortex in both untreated and treated c9ALS cases (Figures 3C, S6C, and S6D). Inclusions localized to ventral horn motor neurons and cortical layers 2 and 5. Poly(GP) immunoassays showed comparable abundance between groups, except for lower poly(GP) in the spinal cords of treated cases (Figures 3D and S6E). Poly(GA) was undetectable in spinal cord by immunoassay but not changed in the motor or frontal cortex between drug-naive and BIIB078-treated c9ALS cases (Figure S6F). Dual IHC confirmed that DPR inclusions persisted in BIIB078-positive cells (Figure S6G).

Mislocalization, hyperphosphorylation, and aggregation of TDP-43 are characteristic pathologies of ALS and frontotemporal lobar degeneration (FTLD) with TDP-43 pathology.[35] We quantified phosphorylated TDP-43 (pTDP-43) abundance in the spinal cord, motor cortex, and frontal cortex and found no differences between drug-naive and BIIB078-treated cases (Figures 3E and S6H). We also quantified truncated *STMN2* (t*STMN2*) expression, a surrogate measure for loss of nuclear TDP-43 function[36,37] and found no difference between drug-naive and BIIB078-treated cases (Figures 3F and S6I).

## Global proteomic changes in c9ALS spinal cord are not normalized by BIIB078

TMT-MS of 34 lumbar spinal cords reliably quantified 9,016 proteins (Figure 4A). We found a substantial number of differentially abundant proteins (DAPs) between both drug-naive and BIIB078-treated c9ALS and non-ALS controls (Figures 4B and 4C; Table S2). Proteomic changes in drug-naive and BIIB078 c9ALS were highly concordant ($R = 0.8$; $p$ value = $2.2 \times 10^{-16}$), with considerable overlap of DAPs; 1,748 DAPs found in BIIB078-treated cases were observed in drug-naive cases (Figures 4B, 4C, and S7A). CNS cell-type-specific proteomic signatures consistent with neuronal loss and reactive gliosis (Table S2),[38] including decreased neuronal and oligodendrocyte markers and increased astrocyte and microglial markers, were observed in c9ALS compared with control, but these were not altered by BIIB078 treatment (Figures 4D, 4E, S7B, and S7C).

## RNase T2 and DNase II are upregulated in BIIB078-treated spinal cords and correlate with BIIB078 concentration

The number and effect size of DAPs between drug-naive and BIIB078-treated c9ALS cases were less than either group compared with controls (Figure 4F). However, in response to BIIB078, several DAPs were upregulated, including the serine/threonine-protein phosphatase 2A regulatory subunit B" subunit

(H and I) Quantification of BIIB078 concentration in spinal cord (H) and motor cortex (I) from control, drug-naive c9ALS, and BIIB078-treated c9ALS cases. Spinal cord: $n = 6$ control, $n = 8$ drug-naive c9ALS, $n = 6$ BIIB078-treated c9ALS cases. Motor cortex: $n = 6$ control, $n = 10$ drug-naive c9ALS, $n = 6$ BIIB078-treated c9ALS cases.

(J) Relative BIIB078 concentrations across various brain regions, normalized to spinal cord values ($n = 6$ cases per region).

(K) Heatmap showing Kendall $\tau$ rank correlation of BIIB078 concentration and dosing parameters across brain regions. L.D., last dose.

See Figures S4 and S5.

Please cite this article in press as: McEachin et al., Molecular impact of antisense oligonucleotide therapy in *C9orf72*-associated ALS, Cell (2025), https://doi.org/10.1016/j.cell.2025.07.045



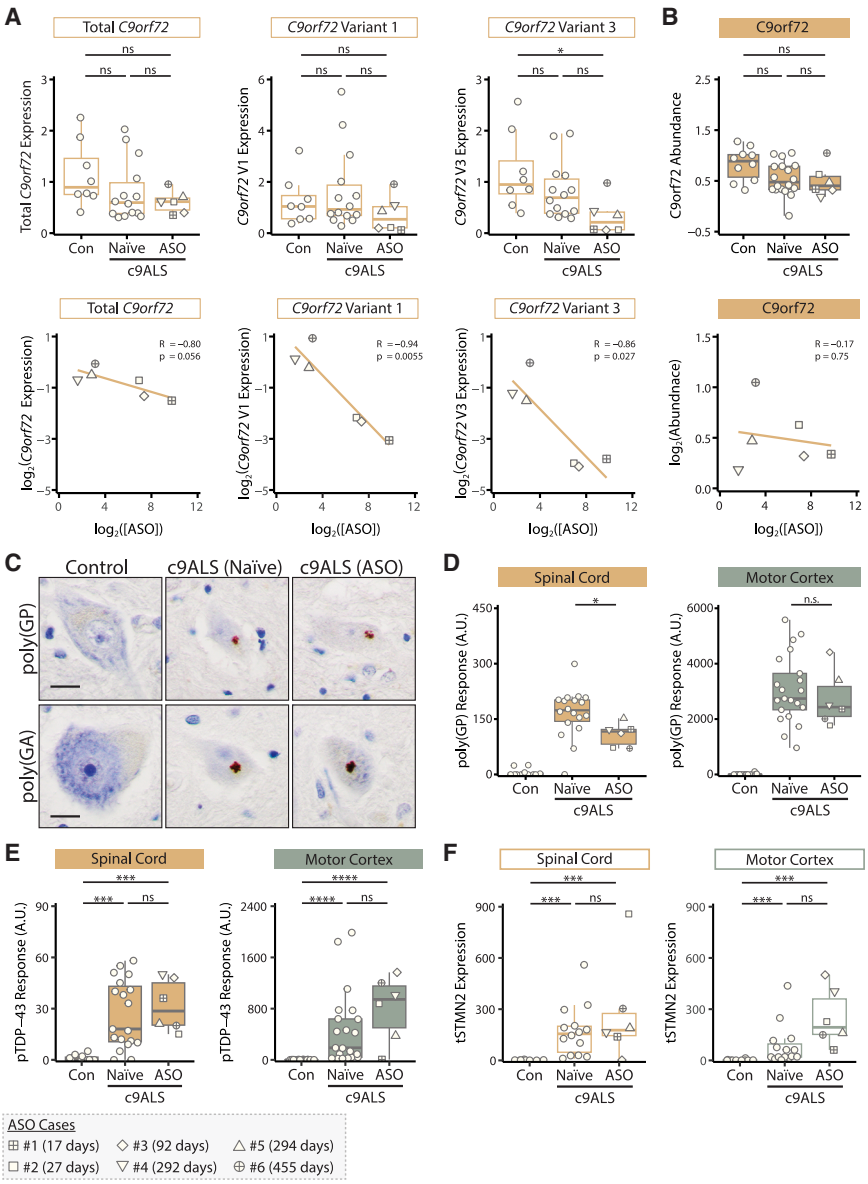


**Figure 3. *C9orf72*-associated neuropathology persists in the CNS of BIIB078-treated cases**

(A) Top: qPCR analysis for total, variant 1 (V1), and variant 3 (V3) *C9orf72* transcripts. Bottom: correlation between *C9orf72* transcript expression and BIIB078 ASO concentration. $n = 8$ control, $n = 14$ drug-naive c9ALS (Naive), $n = 6$ BIIB078-treated c9ALS cases (ASO).

(B) Top: total C9orf72 protein abundance as measured by TMT-MS. Bottom: correlation between C9orf72 protein abundance and BIIB078 ASO concentration. $n = 10$ control, $n = 18$ drug-naive c9ALS, $n = 6$ BIIB078-treated c9ALS cases.

(C) IHC detection of poly(GP) inclusions in the spinal cord of drug-naive and BIIB078-treated cases. Scale bar, 30 μm.

(D) Quantification of poly(GP) abundance via MSD immunoassay in the spinal cord, and motor cortex shows abundant poly(GP) DPRs in drug-naive and BIIB078-treated c9ALS cases. Only comparisons between drug-naive and BIIB078-treated c9ALS cases were considered; two-sided Mann-Whitney test. Spinal cord: $n = 11$ control, $n = 18$ drug-naive c9ALS, $n = 6$ BIIB078-treated c9ALS cases. Motor cortex: $n = 17$ control, $n = 21$ drug-naive c9ALS, $n = 6$ BIIB078-treated c9ALS cases.

(E) Quantification of pTDP-43 abundance via MSD immunoassay in the spinal cord and motor cortex of control, drug-naive c9ALS, and BIIB078-treated cases. Spinal cord: $n = 11$ control, $n = 18$ drug-naive c9ALS, $n = 6$ BIIB078-treated c9ALS cases. Motor cortex: $n = 17$ control, $n = 21$ drug-naive c9ALS, $n = 6$ BIIB078-treated c9ALS cases.

(F) qPCR analysis of truncated *STMN2* (t*STMN2*) expression in spinal cord and motor cortex. Spinal cord: $n = 8$ control, $n = 14$ drug-naive c9ALS, $n = 6$ BIIB078-treated c9ALS cases. Motor cortex: $n = 11$ control, $n = 16$ drug-naive c9ALS, $n = 6$ BIIB078-treated c9ALS cases.

In (A), (B), and (D)–(F), Kruskal-Wallis test followed by Conover-Iman *post hoc* comparisons with Bonferroni correction. $^{*}p < 0.05$, $^{**}p < 0.01$, $^{***}p < 0.001$, $^{****}p < 0.0001$.

See Figure S6.

alpha (PPP2R3A) and the ribonucleases ribonuclease T2 (RNASET2; RNase T2) and deoxyribonuclease-2-alpha (DNASE2; DNase II), or downregulated, including calsequestrin-2 (CASQ2) and LBH domain-containing protein 2 (LBHD2) (Figures 4F and 4G). Several DAPs were strongly correlated with ASO concentration, notably RNase T2 (R = 0.96) and DNase II (R = 0.96) (Figures 4H and 4I; Table S2). Since RNase T2 and DNase II are lysosomal proteins with optimal activity at pH 4–6,[39,40] we assessed whether the upregulation and correlation of these proteins were due to a general increase in lysosomal proteins. Compared with established lysosomal proteins[41] (Table S2), RNase T2 and DNase II were more strongly correlated with BIIB078 tissue concentration and robustly upregulated in BIIB078-treated c9ALS cases (Figures S7D and S7E).

## MOE modifications confer resistance to RNase T2-mediated cleavage of BIIB078

We investigated whether RNase T2 can cleave BIIB078. Cleavage assays were performed by incubating BIIB078 with recombinant RNase T2, followed by urea-PAGE analysis (Figure S8A). BIIB078 (“ASO”) was resistant to RNase T2 cleavage, whereas RNA40, a known substrate of RNase T2,[42] was efficiently cleaved (Figure S8B). As a gapmer ASO, BIIB078 is composed of both ribose and deoxyribose sugars, with its ribose residues modified to contain MOE groups. To systematically assess the contribution of each modification to the resistance of BIIB078 to RNase T2 cleavage, we generated several oligonucleotides based on the BIIB078 sequence (Figure S8A). An unmodified BIIB078 oligonucleotide composed of only

Please cite this article in press as: McEachin et al., Molecular impact of antisense oligonucleotide therapy in *C9orf72*-associated ALS, Cell (2025), https://doi.org/10.1016/j.cell.2025.07.045



CellPress
OPEN ACCESS

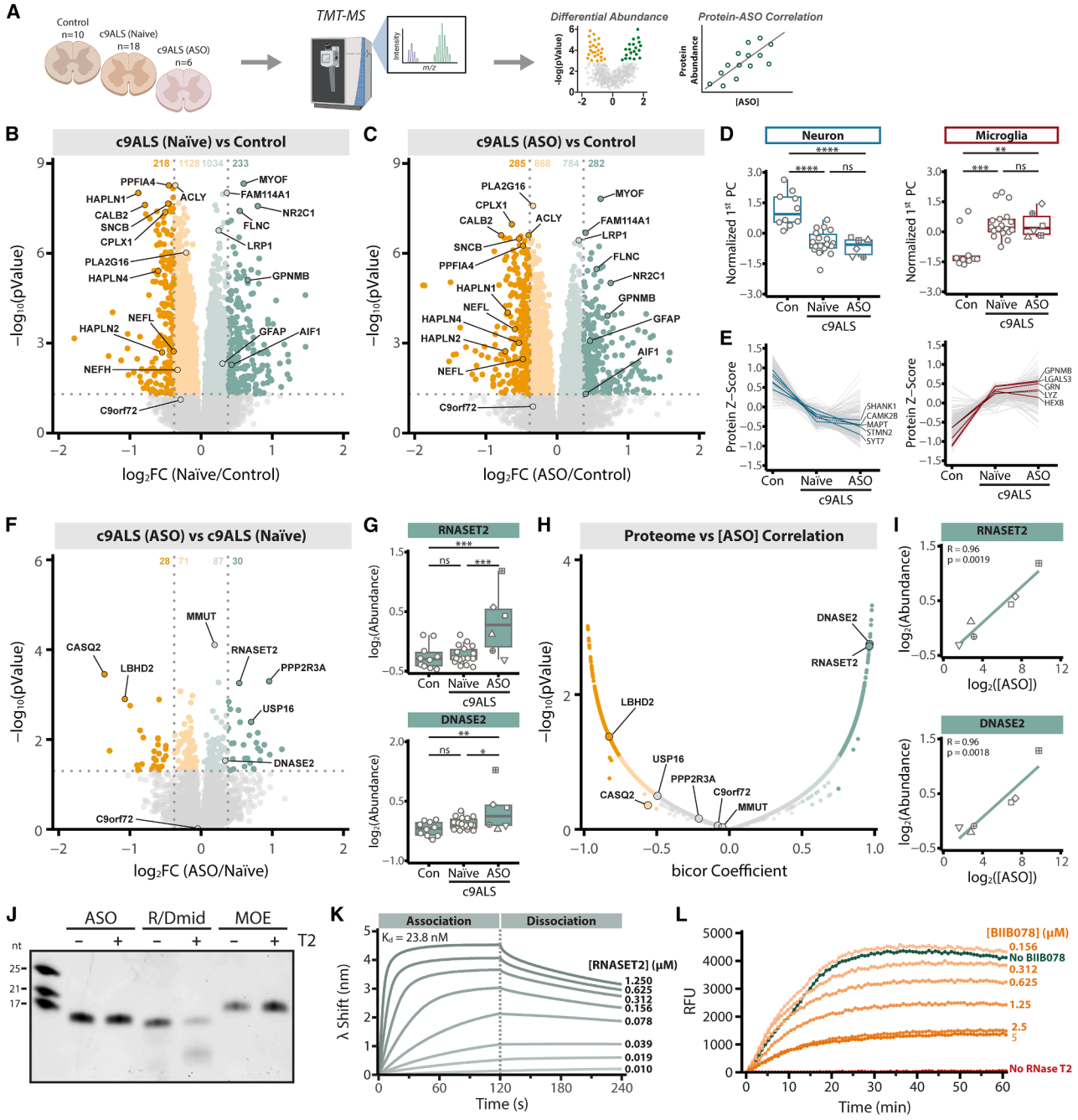


**Figure 4. Global proteomic analysis in spinal cord tissue revealed significant changes in c9ALS cases that were not corrected following BIIB078 treatment**

(A) Schematic of TMT-MS experimental workflow for protein assessment in spinal cord of control ($n = 10$), drug-naive c9ALS (naive; $n = 18$), and BIIB078-treated c9ALS cases (ASO; $n = 6$).

(B and C) Volcano plots displaying $\log_2$FC ($x$ axis) vs. $-\log_{10}$ Tukey's HSD-corrected $p$ values ($y$ axis) comparing (B) drug-naive c9ALS vs. control cases and (C) BIIB078-treated c9ALS vs. control cases. Vertical dotted lines indicate $\log_2$FC = ±0.378 (1.3-fold change).

(D) Boxplots of $Z$ score-normalized eigenprotein values (first principal component) representing variance in curated cell-type marker proteins.[38]

(E) Line plots of $Z$ scored individual protein abundances from the respective cell-type marker list; dotted black line represent mean $Z$ scored value across proteins.

(F) Volcano plots displaying $\log_2$FC ($x$ axis) vs. $-\log_{10}$ Tukey's HSD-corrected $p$ values ($y$ axis) comparing BIIB078-treated vs. drug-naive c9ALS cases.

(G) Boxplots showing abundance of RNase T2 and DNase II across all samples.

(H) Volcano plot showing the biweight midcorrelation coefficient ($x$ axis) vs. the $-\log_{10} p$ value ($y$ axis) between protein abundances and $\log_2$ BIIB078 spinal cord concentration ($n = 6$ BIIB078-treated c9ALS cases).

*(legend continued on next page)*

Please cite this article in press as: McEachin et al., Molecular impact of antisense oligonucleotide therapy in *C9orf72*-associated ALS, Cell (2025), https://doi.org/10.1016/j.cell.2025.07.045



ribonucleotides, but lacking deoxyribonucleotides, was cleaved by RNase T2; substituting uridine with 5-methyluridine, a modification used in BIIB078, did not prevent RNase T2 cleavage (Figure S8C). An unmodified gapmer oligonucleotide ("R/Dmid") exhibited partial cleavage, indicating that the ribonucleotide wings of BIIB078 are susceptible to RNase T2 cleavage (Figure 4J). However, the incorporation of MOE modifications on all ribonucleotides rendered the BIIB078-derived sequence resistant to RNase T2 cleavage (Figure 4J).

### BIIB078 binding modulates RNase T2 cleavage kinetics

Although the unmodified ribonucleotide version of BIIB078 is an RNase T2 substrate, the modified BIIB078 was not cleaved. We used bio-layer interferometry (BLI) to determine whether the fully modified BIIB078 is still bound by RNase T2. Incubation of recombinant RNase T2 with a biotinylated BIIB078 ASO immobilized on a streptavidin sensor produced a concentration-dependent response signal (9.8 nM–1.25 μM) (Figure 4K), indicating direct binding. BIIB078 exhibited a strong affinity for RNase T2, with an apparent dissociation constant ($K_d$) = 23.8 nM (Figure 4K). We thus hypothesized that binding of BIIB078 to RNase T2 would decrease its catalytic activity against other substrates. To test this, we performed competitive cleavage assays in which recombinant RNase T2 was preincubated with increasing concentrations of BIIB078, followed by the addition of a fluorogenic RNA40 oligonucleotide. Urea-PAGE analysis revealed a BIIB078 concentration-dependent shift in cleavage patterns (Figure S8D). In addition, a fluorescence-quenched oligoribonucleotide from a commercial nuclease assay demonstrated that increasing BIIB078 concentrations robustly reduced RNase T2 cleavage efficiency (Figures 4L and S8E).

## DISCUSSION

In this study, we demonstrate that intrathecal administration results in widespread, sustained distribution of BIIB078 throughout the CNS, including the spinal cord and motor cortex, key regions affected in disease, for over a year after the last dose. Importantly, c9ALS-associated pathologies including DPRs and pTDP-43 persisted, and global spinal cord proteomic changes in c9ALS patients were not normalized following BIIB078 treatment.

We measured BIIB078 concentration in the CSF at all dosing time points. At each visit, CSF was collected immediately prior to receiving BIIB078; thus, CSF measurements represent ASO concentration at the nadir of each dosing interval. An initial spike in BIIB078 concentration was observed during the loading dose phase, followed by a drop in concentration at the next dose approximately 1 month later. For several cases, BIIB078 concentration remained stable or continued to decrease with subsequent maintenance doses. Only case #6 demonstrated a clear upward trend in BIIB078 CSF concentration with continued dosing. Why BIIB078 concentration increased with subsequent doses in only one case is perplexing; however, a stable or even decreasing CSF ASO concentration in the other cases could represent greater ASO uptake into the parenchyma.

In five cases, CSF poly(GP) was lower at the final measurement, compared with baseline. However, poly(GP) abundance fluctuated from baseline by as much as ~26%, even in patients treated with placebo prior to transitioning to active drug during the open-label extension (cases #4 and #8). Time intervals between poly(GP) measurements were relatively short (2–4 weeks), which may have contributed to the observed fluctuations in poly(GP) abundance. In comparison to CSF, poly(GP) and poly(GA) in CNS tissues were not robustly different between BIIB078-treated and drug-naive c9ALS cases. Only in the spinal cord did poly(GP) show reduced abundance, compared with the drug-naive c9ALS group, which may be related to proximity of dosing to spinal cord tissue. This discrepancy between CSF and tissue measurements implies a less than direct relationship between target engagement and CNS pathology.

Detection and internalization of BIIB078 in CNS parenchyma, coupled with an overall but variable reduction in CSF poly(GP), suggest engagement with $G_4C_2$ repeat-containing transcripts. However, no consistent reduction in total or variant-specific *C9orf72* transcripts was observed in the spinal cord or motor cortex. Three cases with the highest BIIB078 tissue concentrations exhibited markedly lower *C9orf72* transcript V1/V3 expression in the spinal cord, and transcript abundance strongly correlated with BIIB078 concentration, suggesting that a threshold concentration may be required for robust target engagement. The correlation between *C9orf72* V1/V3 expression and BIIB078 concentration was absent in the motor cortex, where BIIB078 concentrations were lower than in the spinal cord.

Although clinical-pathological correlations were limited by the small number of patients, there were no observable correlations between CSF poly(GP) and either ALSFRS-R scores or CSF neurofilament proteins, data that are consistent with prior findings.[24,43] As an example, one patient (case #6) who showed the most pronounced reduction in poly(GP) (77.6% reduction) and an increase in CSF neurofilament did not show a parallel response to change in ALSFRS-R score. This was the only case that exhibited an increasing concentration of BIIB078 in the CSF that inversely correlated with poly(GP) abundance. Despite a remarkable reduction of poly(GP) in the CSF, case #6 had the lowest BIIB078 concentration at autopsy, although it is important to consider the long interval between poly(GP) measurements at last CSF collection and autopsy. The other

(I) Scatterplots showing strong correlations between RNase T2 and DNase II protein abundance and BIIB078 concentration in the spinal cord ($n$ = 6 BIIB078-treated c9ALS cases).
(J) Urea-PAGE analysis of BIIB078-derived oligo(ribo)nucleotides with recombinant RNase T2. Schematic of oligo(ribo)nucleotides tested provided in Figure S8A.
(K) BLI sensorgrams showing BIIB078 interaction with RNase T2 at varying concentrations.
(L) Fluorescence assay measuring FAM-labeled fluorescence-quenched oligoribonucleotide (500 nM) by RNase T2 (5 nM) with increasing BIIB078 concentrations over 60 min. RFU, relative fluorescence units. Uncropped gel images provided in Data S2.
In (D) and (H), $^{*}p < 0.05$, $^{**}p < 0.01$, $^{***}p < 0.001$, $^{****}p < 0.0001$, ANOVA followed by Tukey's HSD multiple comparison test.
See Figures S7 and S8.

Please cite this article in press as: McEachin et al., Molecular impact of antisense oligonucleotide therapy in *C9orf72*-associated ALS, Cell (2025), https://doi.org/10.1016/j.cell.2025.07.045



cases are informative, albeit to a lesser extent, and suggest that robust delivery of BIIB078 to CNS tissue and reduction of CSF poly(GP) does not necessarily correlate with a reduction of DPRs in tissue nor with a positive clinical response.

The immunogenicity of ASO therapeutics depends on sequence and chemical modifications.[44–47] However, since the CNS is immunologically restrictive, intrathecal ASO delivery is thought to mitigate immunogenic risk. Nonetheless, several cytokines were increased in response to BIIB078, suggesting engagement of immune-related pathways. Notably, CCL26 (eotaxin-3) exhibited the most robust and sustained increase across all cases. Like other members of the eotaxin family, CCL26 signals through C-C chemokine receptor type 3 (CCR3)[48]; it has also been shown to be a functional ligand for other receptors including CX3C chemokine receptor 1 (CX3CR1).[49] A role for CCL26 in the recruitment of leukocytes via the CCL26-CCR3 axis has been shown for several allergic diseases such as eosinophilic esophagitis[50]; however, there are limited studies examining the role of CCL26 in neurodegenerative diseases.[51] It is possible that these cytokine changes could influence disease progression or treatment efficacy. Evaluating CCL26 responses in other intrathecally delivered ASO therapies will provide critical insight into the broader relevance of CCL26 in these treatments. These findings contribute to our understanding of innate immune responses in the human CNS following ASO administration and offer an important framework for pharmacodynamic monitoring of immune system engagement during future clinical trials.

RNase T2 is a lysosomal endoribonuclease that specifically cleaves single-stranded RNA (ssRNA) with a preference for adenosine and uracil[52] and optimal catalytic activity at an acidic pH.[39,40,52] While several uptake pathways have been identified for ASOs,[53] once internalized, ASOs have been shown to localize to lysosomes.[54] Thus, it is plausible that BIIB078 is a substrate for RNase T2 and DNase II. However, owing to backbone and nucleoside modifications, BIIB078 is resistant to cleavage by RNase T2. Nevertheless, BIIB078 interacts with RNase T2, leading us to hypothesize that BIIB078 binding can inhibit RNase T2 activity, as supported by our *in vitro* data. The BIIB078 concentrations needed to inhibit RNase T2 activity in our cleavage assays are comparable to those measured in bulk tissue from BIIB078-treated cases (e.g., case # 1); it is possible that local concentrations within lysosomes are even higher. RNase T2 is involved in innate immunity and mediates Toll-like receptor 8 (TLR8) signaling in response to ssRNA pathogens.[42] Supporting its role in immunity, recessive loss-of-function mutations in *RNASET2* result in cystic leukoencephalopathy.[55] Although not necessarily relevant to the outcome of this trial, it is intriguing to consider that inhibition of RNase T2 by this ASO could dampen innate immune responses to such pathogens. The observed upregulation of RNase T2 may represent a protective response to the cellular accumulation of BIIB078, sequestering BIIB078 in lysosomes, rendering it non-functional.

Overall, this study resolves important knowledge gaps in our understanding of BIIB078 distribution, efficacy, and inflammatory responses in CNS tissue. Although the failure of BIIB078 to provide a clinical benefit[28] might suggest that sense strand gain-of-function mechanisms do not underlie neurodegeneration in c9ALS/FTD, abandoning efforts to target $G_4C_2$ repeat-containing transcripts may be premature. Our data show that despite broad distribution throughout the CNS, BIIB078 did not in fact adequately suppress $G_4C_2$-related pathobiology in tissue. Our integrated proteomics approach across CNS tissue and CSF provides a framework for molecular assessments in future ASO clinical studies, offering valuable insights that will help guide the design and execution of upcoming trials.

## Limitations of the study

A limitation of this study is that we were unable to assess *C9orf72* expression and DPR abundance in tissue before and after BIIB078 treatment, as only postmortem tissue was available. However, the diverse sample cohort, which varied in dosing schemes, total dose administered, and time interval between the last dose and autopsy, allowed us to get a broader picture of BIIB078 distribution and pathological efficacy throughout the CNS. A second limitation is the number of BIIB078-treated cases, which reflects the limited availability of postmortem cases from patients enrolled in this clinical trial. While this study focused on BIIB078, it will be important to determine whether key findings, particularly pharmacodynamic biomarkers and proteomic changes, such as CCL26 and RNase T2, are also observed in other ASO treatments.

## RESOURCE AVAILABILITY

### Lead contact

Requests for further information should be directed to the lead contact, Zachary McEachin (zmceach@emory.edu).

### Materials availability

All materials from this study are included in the article and key resources table. Any material that can be shared will be made available upon request. Tissue specimens have limited availability.

### Data and code availability

The MS proteomics raw files, metadata, and data analysis files are deposited to the ProteomeXchange Consortium (https://www.proteomexchange.org/; accession number PRIDE: PXD055796) and Synapse (https://www.synapse.org/Synapse:syn59424246).

## ACKNOWLEDGMENTS

We are grateful to patients and their families for their participation in the clinical trial and donation of postmortem tissue. We thank Jeffrey Rothstein and Alyssa Coyne for kindly providing the anti-ASO antibody, Gary Bassell and Jie Jiang for insightful discussions, and Mai Thayer for helpful discussions regarding establishment of the POE assay. This work was supported by NIH 1R01NS137434 (Z.T.M.), NIH 5P01NS084974 (L.P., J.D.G., and T.F.G.), NIH P30AG066511 (M.G. and J.D.G.), The AFTD Pathways for Hope Pilot Grant (Z.T.M.), and institutional support from the Laboratory for Translational Cell Biology, Emory University (Z.T.M.).

## AUTHOR CONTRIBUTIONS

Z.T.M. and J.D.G. conceived the project. Z.T.M. supervised, designed, and coordinated the project. Z.T.M., M.C., S.A.S., U.S., E.B.D., N.R., T.F.G., N.T.S., and J.D.G. curated, analyzed, and interpreted data. Z.T.M., M.C., and S.A.S. performed immunohistochemistry, ISH, and qPCR. Z.T.M., S.A.S., U.S., and T.F.G. performed Mesoscale Discovery (MSD) immunoassays. Z.T.M., W.J.K., and C.H. analyzed NULISA data. D.M.D. and L.P. processed samples for and performed MS. P.M. and T.K. produced recombinant RNase T2

proteins. Z.T.M. and T.K. performed BLI experiments. Z.T.M., E.B.D., A.S., A. N.T., and N.T.S. analyzed proteomic data. Y.L. and T.E.G. performed mouse ICV injections. E.V.T., T.K., E.I., M.G., S.F.R., M.D., C.F., D.W.D., L.P., B.O., and J.D.G. provided patient samples and associated genetic/clinical data. E. V.T., M.G., K.M.K., N.R., E.A., and S.A. provided technical support. Z.T.M., L.P., T.F.G., N.T.S., and J.D.G. oversaw project administration and funding acquisition. Z.T.M. wrote the initial manuscript draft. Z.T.M., M.C., S.A.S., E. V.T., N.R., L.P., T.F.G., N.T.S., and J.D.G. revised and edited the manuscript.

## DECLARATION OF INTERESTS

N.T.S., Z.T.M., and J.D.G. are co-founders of StitchRx. N.T.S. and D.M.D. are co-founders and consultants of Emtherapro and Arc Proteomics.

## STAR★METHODS

Detailed methods are provided in the online version of this paper and include the following:

- KEY RESOURCES TABLE
- METHOD DETAILS
  - Lysate preparation
  - miRNAscope in situ hybridization (ISH) Assay
  - CSF Neurofilament (NfL) Immunoassay
  - Meso-Scale Discovery (MSD) immunoassay (pTDP-43, polyGP, polyGA)
  - NULISAseq Assay
  - Immunohistochemistry
  - Plate-based oligonucleotide electro-chemiluminescent (POE) immunoassay
  - RNA extraction and quantitative reverse transcription with PCR (RT-PCR)
  - Neonatal Intracerebroventricular (ICV) Injections
  - Production and purification of recombinant RNase T2 protein
  - RNase T2 Cleavage Assays
  - Nuclease Competition Assay
  - Bio-layer interferometry (BLI) binding assays
  - Tissue Homogenization and Protein Digestion
  - Isobaric Tandem Mass Tag (TMT) Peptide Labeling
  - High-pH Off-line Fractionation
  - Liquid Chromatography Tandem Mass Spectrometry
  - Database Searches and Protein Quantification
  - Bioinformatics processing and statistical analysis
- QUANTIFICATION AND STATISTICAL ANALYSIS

## SUPPLEMENTAL INFORMATION

Supplemental information can be found online at https://doi.org/10.1016/j.cell.2025.07.045.

Received: September 11, 2024
Revised: March 20, 2025
Accepted: July 30, 2025

## REFERENCES

1. Hardiman, O., Al-Chalabi, A., Chio, A., Corr, E.M., Logroscino, G., Robberecht, W., Shaw, P.J., Simmons, Z., and van den Berg, L.H. (2017). Amyotrophic lateral sclerosis. Nat. Rev. Dis. Primers *3*, 17071. https://doi.org/10.1038/nrdp.2017.71.
2. DeJesus-Hernandez, M., Mackenzie, I.R., Boeve, B.F., Boxer, A.L., Baker, M., Rutherford, N.J., Nicholson, A.M., Finch, N.A., Flynn, H., Adamson, J., et al. (2011). Expanded GGGGCC hexanucleotide repeat in noncoding region of C9ORF72 causes chromosome 9p-linked FTD and ALS. Neuron *72*, 245–256. https://doi.org/10.1016/j.neuron.2011.09.011.
3. Renton, A.E., Majounie, E., Waite, A., Simón-Sánchez, J., Rollinson, S., Gibbs, J.R., Schymick, J.C., Laaksovirta, H., van Swieten, J.C., Myllykangas, L., et al. (2011). A hexanucleotide repeat expansion in C9ORF72 is the cause of chromosome 9p21-linked ALS-FTD. Neuron *72*, 257–268. https://doi.org/10.1016/j.neuron.2011.09.010.
4. Balendra, R., and Isaacs, A.M. (2018). C9orf72-mediated ALS and FTD: multiple pathways to disease. Nat. Rev. Neurol. *14*, 544–558. https://doi.org/10.1038/s41582-018-0047-2.
5. Lee, Y.B., Chen, H.J., Peres, J.N., Gomez-Deza, J., Attig, J., Stalekar, M., Troakes, C., Nishimura, A.L., Scotter, E.L., Vance, C., et al. (2013). Hexanucleotide repeats in ALS/FTD form length-dependent RNA foci, sequester RNA binding proteins, and are neurotoxic. Cell Rep. *5*, 1178–1186. https://doi.org/10.1016/j.celrep.2013.10.049.
6. Cooper-Knock, J., Walsh, M.J., Higginbottom, A., Robin Highley, J., Dickman, M.J., Edbauer, D., Ince, P.G., Wharton, S.B., Wilson, S.A., Kirby, J., et al. (2014). Sequestration of multiple RNA recognition motif-containing proteins by C9orf72 repeat expansions. Brain *137*, 2040–2051. https://doi.org/10.1093/brain/awu120.
7. Donnelly, C.J., Zhang, P.W., Pham, J.T., Haeusler, A.R., Mistry, N.A., Vidensky, S., Daley, E.L., Poth, E.M., Hoover, B., Fines, D.M., et al. (2013). RNA toxicity from the ALS/FTD C9ORF72 expansion is mitigated by antisense intervention. Neuron *80*, 415–428. https://doi.org/10.1016/j.neuron.2013.10.015.
8. Sareen, D., O'Rourke, J.G., Meera, P., Muhammad, A.K.M.G., Grant, S., Simpkinson, M., Bell, S., Carmona, S., Ornelas, L., Sahabian, A., et al. (2013). Targeting RNA Foci in iPSC-Derived Motor Neurons from ALS Patients with a C9ORF72 Repeat Expansion. Sci. Transl. Med. *5*, 208ra149. https://doi.org/10.1126/scitranslmed.3007529.
9. Zhang, K., Donnelly, C.J., Haeusler, A.R., Grima, J.C., Machamer, J.B., Steinwald, P., Daley, E.L., Miller, S.J., Cunningham, K.M., Vidensky, S., et al. (2015). The C9orf72 repeat expansion disrupts nucleocytoplasmic transport. Nature *525*, 56–61. https://doi.org/10.1038/nature14973.
10. Mori, K., Weng, S.M., Arzberger, T., May, S., Rentzsch, K., Kremmer, E., Schmid, B., Kretzschmar, H.A., Cruts, M., Van Broeckhoven, C., et al. (2013). The C9orf72 GGGGCC repeat is translated into aggregating dipeptide-repeat proteins in FTLD/ALS. Science *339*, 1335–1338. https://doi.org/10.1126/science.1232927.
11. Gendron, T.F., Bieniek, K.F., Zhang, Y.J., Jansen-West, K., Ash, P.E.A., Caulfield, T., Daughrity, L., Dunmore, J.H., Castanedes-Casey, M., Chew, J., et al. (2013). Antisense transcripts of the expanded C9ORF72 hexanucleotide repeat form nuclear RNA foci and undergo repeat-associated non-ATG translation in c9FTD/ALS. Acta Neuropathol. *126*, 829–844. https://doi.org/10.1007/s00401-013-1192-8.
12. Zu, T., Liu, Y., Bañez-Coronel, M., Reid, T., Pletnikova, O., Lewis, J., Miller, T.M., Harms, M.B., Falchook, A.E., Subramony, S.H., et al. (2013). RAN proteins and RNA foci from antisense transcripts in C9ORF72 ALS and frontotemporal dementia. Proc. Natl. Acad. Sci. USA *110*, E4968–E4977. https://doi.org/10.1073/pnas.1315438110.
13. Zhang, Y.J., Jansen-West, K., Xu, Y.F., Gendron, T.F., Bieniek, K.F., Lin, W.L., Sasaguri, H., Caulfield, T., Hubbard, J., Daughrity, L., et al. (2014). Aggregation-prone c9FTD/ALS poly(GA) RAN-translated proteins cause neurotoxicity by inducing ER stress. Acta Neuropathol. *128*, 505–524. https://doi.org/10.1007/s00401-014-1336-5.
14. Zhang, Y.J., Gendron, T.F., Grima, J.C., Sasaguri, H., Jansen-West, K., Xu, Y.F., Katzman, R.B., Gass, J., Murray, M.E., Shinohara, M., et al. (2016). C9ORF72 poly(GA) aggregates sequester and impair HR23 and nucleocytoplasmic transport proteins. Nat. Neurosci. *19*, 668–677. https://doi.org/10.1038/nn.4272.
15. Zhang, Y.-J., Gendron, T.F., Ebbert, M.T.W., O'Raw, A.D., Yue, M., Jansen-West, K., Zhang, X., Prudencio, M., Chew, J., Cook, C.N., et al. (2018). Poly(GR) impairs protein translation and stress granule dynamics in C9orf72-associated frontotemporal dementia and amyotrophic lateral sclerosis. Nat. Med. *24*, 1136–1142. https://doi.org/10.1038/s41591-018-0071-1.

16. Lee, K.-H., Zhang, P., Kim, H.J., Mitrea, D.M., Sarkar, M., Freibaum, B.D., Cika, J., Coughlin, M., Messing, J., Molliex, A., et al. (2016). C9orf72 Dipeptide Repeats Impair the Assembly, Dynamics, and Function of Membrane-Less Organelles. Cell *167*, 774–788.e17. https://doi.org/10.1016/j.cell.2016.10.002.

17. Boeynaems, S., Bogaert, E., Kovacs, D., Konijnenberg, A., Timmerman, E., Volkov, A., Guharoy, M., De Decker, M., Jaspers, T., Ryan, V.H., et al. (2017). Phase Separation of C9orf72 Dipeptide Repeats Perturbs Stress Granule Dynamics. Mol. Cell *65*, 1044–1055.e5. https://doi.org/10.1016/j.molcel.2017.02.013.

18. Zhang, Y.J., Guo, L., Gonzales, P.K., Gendron, T.F., Wu, Y., Jansen-West, K., O'Raw, A.D., Pickles, S.R., Prudencio, M., Carlomagno, Y., et al. (2019). Heterochromatin anomalies and double-stranded RNA accumulation underlie C9orf72 poly(PR) toxicity. Science *363*, eaav2606. https://doi.org/10.1126/science.aav2606.

19. Milioto, C., Carcolé, M., Giblin, A., Coneys, R., Attrebi, O., Ahmed, M., Harris, S.S., Lee, B.I., Yang, M., Ellingford, R.A., et al. (2024). PolyGR and polyPR knock-in mice reveal a conserved neuroprotective extracellular matrix signature in C9orf72 ALS/FTD neurons. Nat. Neurosci. *27*, 643–655. https://doi.org/10.1038/s41593-024-01589-4.

20. Bennett, C.F. (2019). Therapeutic Antisense Oligonucleotides Are Coming of Age. Annu. Rev. Med. *70*, 307–321. https://doi.org/10.1146/annurev-med-041217-010829.

21. Hu, J., Rigo, F., Prakash, T.P., and Corey, D.R. (2017). Recognition of c9orf72 Mutant RNA by Single-Stranded Silencing RNAs. Nucleic Acid Ther. *27*, 87–94. https://doi.org/10.1089/nat.2016.0655.

22. Hu, J., Liu, J., Li, L., Gagnon, K.T., and Corey, D.R. (2015). Engineering Duplex RNAs for Challenging Targets: Recognition of GGGGCC/CCCCGG Repeats at the ALS/FTD C9orf72 Locus. Chem. Biol. *22*, 1505–1511. https://doi.org/10.1016/j.chembiol.2015.09.016.

23. Lagier-Tourenne, C., Baughn, M., Rigo, F., Sun, S., Liu, P., Li, H.R., Jiang, J., Watt, A.T., Chun, S., Katz, M., et al. (2013). Targeted degradation of sense and antisense C9orf72 RNA foci as therapy for ALS and frontotemporal degeneration. Proc. Natl. Acad. Sci. USA *110*, E4530–E4539. https://doi.org/10.1073/pnas.1318835110.

24. Gendron, T.F., Chew, J., Stankowski, J.N., Hayes, L.R., Zhang, Y.-J., Prudencio, M., Carlomagno, Y., Daughrity, L.M., Jansen-West, K., Perkerson, E.A., et al. (2017). Poly(GP) proteins are a useful pharmacodynamic marker for C9ORF72-associated amyotrophic lateral sclerosis. Sci. Transl. Med. *9*, eaai7866. https://doi.org/10.1126/scitranslmed.aai7866.

25. Jiang, J., Zhu, Q., Gendron, T.F., Saberi, S., McAlonis-Downes, M., Seelman, A., Stauffer, J.E., Jafar-Nejad, P., Drenner, K., Schulte, D., et al. (2016). Gain of Toxicity from ALS/FTD-Linked Repeat Expansions in C9ORF72 Is Alleviated by Antisense Oligonucleotides Targeting GGGGCC-Containing RNAs. Neuron *90*, 535–550. https://doi.org/10.1016/j.neuron.2016.04.006.

26. Liu, Y., Dodart, J.C., Tran, H., Berkovitch, S., Braun, M., Byrne, M., Durbin, A.F., Hu, X.S., Iwamoto, N., Jang, H.G., et al. (2021). Variant-selective stereopure oligonucleotides protect against pathologies associated with C9orf72-repeat expansion in preclinical models. Nat. Commun. *12*, 847. https://doi.org/10.1038/s41467-021-21112-8.

27. Rothstein, J.D., Baskerville, V., Rapuri, S., Mehlhop, E., Jafar-Nejad, P., Rigo, F., Bennett, F., Mizielinska, S., Isaacs, A., and Coyne, A.N. (2023). $G_2C_4$ targeting antisense oligonucleotides potently mitigate TDP-43 dysfunction in human C9orf72 ALS/FTD induced pluripotent stem cell derived neurons. Acta Neuropathol. *147*, 1. https://doi.org/10.1007/s00401-023-02652-3.

28. van den Berg, L.H., Rothstein, J.D., Shaw, P.J., Babu, S., Benatar, M., Bucelli, R.C., Genge, A., Glass, J.D., Hardiman, O., Libri, V., et al. (2024). Safety, tolerability, and pharmacokinetics of antisense oligonucleotide BIIB078 in adults with C9orf72-associated amyotrophic lateral sclerosis: a phase 1, randomised, double blinded, placebo-controlled, multiple ascending dose study. Lancet Neurol. *23*, 901–912. https://doi.org/10.1016/S1474-4422(24)00216-3.

29. Tran, H., Moazami, M.P., Yang, H., McKenna-Yasek, D., Douthwright, C. L., Pinto, C., Metterville, J., Shin, M., Sanil, N., Dooley, C., et al. (2022). Suppression of mutant C9orf72 expression by a potent mixed backbone antisense oligonucleotide. Nat. Med. *28*, 117–124. https://doi.org/10.1038/s41591-021-01557-6.

30. Krishnan, G., Raitcheva, D., Bartlett, D., Prudencio, M., McKenna-Yasek, D.M., Douthwright, C., Oskarsson, B.E., Ladha, S., King, O.D., Barmada, S.J., et al. (2022). Poly(GR) and poly(GA) in cerebrospinal fluid as potential biomarkers for C9ORF72-ALS/FTD. Nat. Commun. *13*, 2799. https://doi.org/10.1038/s41467-022-30387-4.

31. Lu, C.-H., Macdonald-Wallis, C., Gray, E., Pearce, N., Petzold, A., Norgren, N., Giovannoni, G., Fratta, P., Sidle, K., Fish, M., et al. (2015). Neurofilament light chain: A prognostic biomarker in amyotrophic lateral sclerosis. Neurology *84*, 2247–2257. https://doi.org/10.1212/WNL.0000000000001642.

32. Benatar, M., Wuu, J., and Turner, M.R. (2023). Neurofilament light chain in drug development for amyotrophic lateral sclerosis: a critical appraisal. Brain *146*, 2711–2716. https://doi.org/10.1093/brain/awac394.

33. Thayer, M.B., Humphreys, S.C., Chung, K.S., Lade, J.M., Cook, K.D., and Rock, B.M. (2020). POE Immunoassay: Plate-based oligonucleotide electro-chemiluminescent immunoassay for the quantification of nucleic acids in biological matrices. Sci. Rep. *10*, 10425. https://doi.org/10.1038/s41598-020-66829-6.

34. Feng, W., Beer, J.C., Hao, Q., Ariyapala, I.S., Sahajan, A., Komarov, A., Cha, K., Moua, M., Qiu, X., Xu, X., et al. (2023). NULISA: a proteomic liquid biopsy platform with attomolar sensitivity and high multiplexing. Nat. Commun. *14*, 7238. https://doi.org/10.1038/s41467-023-42834-x.

35. Neumann, M., Sampathu, D.M., Kwong, L.K., Truax, A.C., Micsenyi, M.C., Chou, T.T., Bruce, J., Schuck, T., Grossman, M., Clark, C.M., et al. (2006). Ubiquitinated TDP-43 in frontotemporal lobar degeneration and amyotrophic lateral sclerosis. Science *314*, 130–133. https://doi.org/10.1126/science.1134108.

36. Melamed, Z., López-Erauskin, J., Baughn, M.W., Zhang, O., Drenner, K., Sun, Y., Freyermuth, F., McMahon, M.A., Beccari, M.S., Artates, J.W., et al. (2019). Premature polyadenylation-mediated loss of stathmin-2 is a hallmark of TDP-43-dependent neurodegeneration. Nat. Neurosci. *22*, 180–190. https://doi.org/10.1038/s41593-018-0293-z.

37. Klim, J.R., Williams, L.A., Limone, F., Guerra San Juan, I., Davis-Dusenbery, B.N., Mordes, D.A., Burberry, A., Steinbaugh, M.J., Gamage, K.K., Kirchner, R., et al. (2019). ALS-implicated protein TDP-43 sustains levels of STMN2, a mediator of motor neuron growth and repair. Nat. Neurosci. *22*, 167–179. https://doi.org/10.1038/s41593-018-0300-4.

38. Johnson, E.C.B., Carter, E.K., Dammer, E.B., Duong, D.M., Gerasimov, E. S., Liu, Y., Liu, J., Betarbet, R., Ping, L., Yin, L., et al. (2022). Large-scale deep multi-layer analysis of Alzheimer's disease brain reveals strong proteomic disease-related changes not observed at the RNA level. Nat. Neurosci. *25*, 213–225. https://doi.org/10.1038/s41593-021-00999-y.

39. Luhtala, N., and Parker, R. (2010). T2 Family ribonucleases: ancient enzymes with diverse roles. Trends Biochem. Sci. *35*, 253–259. https://doi.org/10.1016/j.tibs.2010.02.002.

40. Evans, C.J., and Aguilera, R.J. (2003). DNase II: genes, enzymes and function. Gene *322*, 1–15. https://doi.org/10.1016/j.gene.2003.08.022.

41. Sleat, D.E., Zheng, H., Qian, M., and Lobel, P. (2006). Identification of sites of mannose 6-phosphorylation on lysosomal proteins. Mol. Cell. Proteomics *5*, 686–701. https://doi.org/10.1074/mcp.M500343-MCP200.

42. Greulich, W., Wagner, M., Gaidt, M.M., Stafford, C., Cheng, Y., Linder, A., Carell, T., and Hornung, V. (2019). TLR8 Is a Sensor of RNase T2 Degradation Products. Cell *179*, 1264–1275.e13. https://doi.org/10.1016/j.cell.2019.11.001.

43. Gendron, T.F., C9ORF72 Neurofilament Study Group, Daughrity, L.M., Heckman, M.G., Diehl, N.N., Wuu, J., Miller, T.M., Pastor, P., Trojanowski, J.Q., Grossman, M., et al. (2017). Phosphorylated neurofilament heavy chain: A biomarker of survival for C9ORF72-associated amyotrophic

lateral sclerosis. Ann. Neurol. *82*, 139–146. https://doi.org/10.1002/ana.24980.

44. Senn, J.J., Burel, S., and Henry, S.P. (2005). Non-CpG-Containing Antisense 2′-Methoxyethyl Oligonucleotides Activate a Proinflammatory Response Independent of Toll-Like Receptor 9 or Myeloid Differentiation Factor 88. J. Pharmacol. Exp. Ther. *314*, 972–979. https://doi.org/10.1124/jpet.105.084004.
45. Shen, W., De Hoyos, C.L., Migawa, M.T., Vickers, T.A., Sun, H., Low, A., Bell, T.A., Rahdar, M., Mukhopadhyay, S., Hart, C.E., et al. (2019). Chemical modification of PS-ASO therapeutics reduces cellular protein-binding and improves the therapeutic index. Nat. Biotechnol. *37*, 640–650. https://doi.org/10.1038/s41587-019-0106-2.
46. Goyenvalle, A., Jimenez-Mallebrera, C., van Roon, W., Sewing, S., Krieg, A.M., Arechavala-Gomeza, V., and Andersson, P. (2023). Considerations in the Preclinical Assessment of the Safety of Antisense Oligonucleotides. Nucleic Acid Ther. *33*, 1–16. https://doi.org/10.1089/nat.2022.0061.
47. Winkle, M., El-Daly, S.M., Fabbri, M., and Calin, G.A. (2021). Noncoding RNA therapeutics — challenges and potential solutions. Nat. Rev. Drug Discov. *20*, 629–651. https://doi.org/10.1038/s41573-021-00219-z.
48. Kitaura, M., Suzuki, N., Imai, T., Takagi, S., Suzuki, R., Nakajima, T., Hirai, K., Nomiyama, H., and Yoshie, O. (1999). Molecular cloning of a novel human CC chemokine (Eotaxin-3) that is a functional ligand of CC chemokine receptor 3. J. Biol. Chem. *274*, 27975–27980. https://doi.org/10.1074/jbc.274.39.27975.
49. Nakayama, T., Watanabe, Y., Oiso, N., Higuchi, T., Shigeta, A., Mizuguchi, N., Katou, F., Hashimoto, K., Kawada, A., and Yoshie, O. (2010). Eotaxin-3/CC chemokine ligand 26 is a functional ligand for CX3CR1. J. Immunol. *185*, 6472–6479. https://doi.org/10.4049/jimmunol.0904126.
50. Blanchard, C., Wang, N., Stringer, K.F., Mishra, A., Fulkerson, P.C., Abonia, J.P., Jameson, S.C., Kirby, C., Konikoff, M.R., Collins, M.H., et al. (2006). Eotaxin-3 and a uniquely conserved gene-expression profile in eosinophilic esophagitis. J. Clin. Invest. *116*, 536–547. https://doi.org/10.1172/JCI26679.
51. Huber, A.K., Giles, D.A., Segal, B.M., and Irani, D.N. (2018). An emerging role for eotaxins in neurodegenerative disease. Clin. Immunol. *189*, 29–33. https://doi.org/10.1016/j.clim.2016.09.010.
52. Campomenosi, P., Salis, S., Lindqvist, C., Mariani, D., Nordström, T., Acquati, F., and Taramelli, R. (2006). Characterization of RNASET2, the first human member of the Rh/T2/S family of glycoproteins. Arch. Biochem. Biophys. *449*, 17–26. https://doi.org/10.1016/j.abb.2006.02.022.
53. Crooke, S.T., Wang, S., Vickers, T.A., Shen, W., and Liang, X.H. (2017). Cellular uptake and trafficking of antisense oligonucleotides. Nat. Biotechnol. *35*, 230–237. https://doi.org/10.1038/nbt.3779.
54. Geary, R.S., Norris, D., Yu, R., and Bennett, C.F. (2015). Pharmacokinetics, biodistribution and cell uptake of antisense oligonucleotides. Adv. Drug Deliv. Rev. *87*, 46–51. https://doi.org/10.1016/j.addr.2015.01.008.
55. Henneke, M., Diekmann, S., Ohlenbusch, A., Kaiser, J., Engelbrecht, V., Kohlschütter, A., Krätzner, R., Madruga-Garrido, M., Mayer, M., Opitz, L., et al. (2009). RNASET2-deficient cystic leukoencephalopathy resembles congenital cytomegalovirus brain infection. Nat. Genet. *41*, 773–775. https://doi.org/10.1038/ng.398.
56. Seifar, F., Fox, E.J., Shantaraman, A., Liu, Y., Dammer, E.B., Modeste, E., Duong, D.M., Yin, L., Trautwig, A.N., Guo, Q., et al. (2024). Large-scale Deep Proteomic Analysis in Alzheimer's Disease Brain Regions Across Race and Ethnicity. Alzheimers Dement. *20*, 8878–8897. https://doi.org/10.1002/alz.14360.
57. Käll, L., Canterbury, J.D., Weston, J., Noble, W.S., and MacCoss, M.J. (2007). Semi-supervised learning for peptide identification from shotgun proteomics datasets. Nat. Methods *4*, 923–925. https://doi.org/10.1038/nmeth1113.
58. Dammer, E.B., Seyfried, N.T., and Johnson, E.C.B. (2023). Batch Correction and Harmonization of -Omics Datasets with a Tunable Median Polish of Ratio. Front. Syst. Biol. *3*, 1092341. https://doi.org/10.3389/fsysb.2023.1092341.
59. Johnson, E.C.B., Dammer, E.B., Duong, D.M., Ping, L., Zhou, M., Yin, L., Higginbotham, L.A., Guajardo, A., White, B., Troncoso, J.C., et al. (2020). Large-scale proteomic analysis of Alzheimer's disease brain and cerebrospinal fluid reveals early changes in energy metabolism associated with microglia and astrocyte activation. Nat. Med. *26*, 769–780. https://doi.org/10.1038/s41591-020-0815-6.
60. Suomi, T., Seyednasrollah, F., Jaakkola, M.K., Faux, T., and Elo, L.L. (2017). ROTS: An R package for reproducibility-optimized statistical testing. PLoS Comput. Biol. *13*, e1005562. https://doi.org/10.1371/journal.pcbi.1005562.

Please cite this article in press as: McEachin et al., Molecular impact of antisense oligonucleotide therapy in *C9orf72*-associated ALS, Cell (2025), https://doi.org/10.1016/j.cell.2025.07.045



CellPress
OPEN ACCESS

## STAR★METHODS

### KEY RESOURCES TABLE

| REAGENT or RESOURCE | SOURCE | IDENTIFIER |
|---|---|---|
| Antibodies | | |
| Mouse monoclonal anti-poly(GP) | Target ALS | Cat#: TALS 828.179; RRID: AB_2753317 |
| Mouse monoclonal anti-poly(GA), clone 5E9 | Millipore Sigma | Cat#: MABN889; RRID: AB_2728663 |
| Rabbit polyclonal anti-TDP-43 (C-terminal) | ProteinTech | Cat#: 12892-1-AP; RRID: AB_2200505 |
| Mouse monoclonal anti-phosphorylated TDP-43 (S409/410) | CosmoBio | Cat#: CAC-TIP-PTD-M01; RRID: AB_1961900 |
| Sheep polyclonal anti-Digoxygenin | Novus Biologicals | Cat#: NB100-65495; RRID: AB_963219 |
| Rabbit anti-ASO | Gift from Jeffrey Rothstein | N/A |
| Biological samples | | |
| ALS Postmortem Tissue (see Table S1) | Emory University; Mayo Clinic Jacksonville | N/A |
| ALS Cerebrospinal Fluid (see Table S1) | Emory University | N/A |
| Chemicals, peptides, and recombinant proteins | | |
| Envision HRP anti-mouse | Dako/Agilent | Cat#: K400111-2 |
| Envision HRP anti-rabbit | Dako/Agilent | Cat#: K400311-2 |
| DAB+ Liquid Kit | Dako/Agilent | Cat#: K346811-2 |
| Serum-free Protein Block | Dako/Agilent | Cat#: X090930-2 |
| Dual Endogenous Enzyme Block | Dako/Agilent | Cat#: S200389-2 |
| Antibody Diluent | Dako/Agilent | Cat#: S080983-2 |
| Sulfuric Acid 0.3M | Dako/Agilent | Cat#: GC20330-5 |
| EnVision FLEX HRP Magenta Substrate Chromogen System | Dako/Agilent | Cat#: GV92511-2 |
| ImmPACT® SG Substrate Kit, Peroxidase (HRP) | Vector Laboratories | Cat#: SK-4705 |
| Methyl Green Counterstain | Vector Laboratories | Cat#: H-3402-500 |
| Proteinase K | Thermo Fisher Scientific | Cat#: EO0491 |
| SuperBlock Blocking Buffer | Thermo Fisher Scientific | Cat#: 37580 |
| Taqman Advanced MasterMix | Thermo Fisher Scientific | Cat#: 4444964 |
| HALT™ Protease Inhibitor Cocktail | Thermo Fisher Scientific | Cat#: 87786 |
| Trypsin, Mass Spectrometry-grade | Thermo Fisher Scientific | Cat#: 90059 |
| ExpiFectamine™ 293 Transfection Kit | Thermo Fisher Scientific | Cat#: A14525 |
| TMTpro 16plex Label Reagent Set | Thermo Fisher Scientific | Cat#: A44520; Lot#: YA357799 |
| TMTpro 1134C & TMTpro 135N Label Reagents | Thermo Fisher Scientific | Cat#: A52846; Lot#: YB370079 |
| Lysyl Endopeptidase, Mass Spectrometry-grade | Fujifilm/Wako | Cat#: 125-05061 |
| Histo-Clear II | National Diagnostics | Cat#: HS-202 |
| MSD Blocker A Kit | Mesoscale Discovery | Cat#: R93AA-2 |
| MSD GOLD Read Buffer A | Mesoscale Discovery | Cat#: R92TG-1 |
| MSD GOLD Read Buffer T (4x) | Mesoscale Discovery | Cat#: R92TC-2 |
| Recombinant Human RNASET2 | This paper | N/A |
| Recombinant Human RNASET2 H65/118F Mutant | This paper | N/A |
| SYBR Gold Nucleic Acid Gel Stain | Thermo Fisher Scientific | Cat#: S11494 |
| TBE-Urea Sample Buffer (2x) | Thermo Fisher Scientific | Cat#: LC6876 |
| TBE Running Buffer (5X) | Thermo Fisher Scientific | LC6675 |
| 15% TBE-Urea Gel | Thermo Fisher Scientific | EC6885BOX |

(*Continued on next page*)

Please cite this article in press as: McEachin et al., Molecular impact of antisense oligonucleotide therapy in *C9orf72*-associated ALS, Cell (2025), https://doi.org/10.1016/j.cell.2025.07.045



***Continued***

| REAGENT or RESOURCE | SOURCE | IDENTIFIER |
|---|---|---|
| **Critical commercial assays** | | |
| Custom BIIB078 ASO miRNAscope Probe | Bio-Techne | Probe ID: SR-ASO-Hs-C9orf72-S1 |
| miRNAscope™ HD Detection Reagents - RED | Bio-Techne | Cat#: 324510 |
| RNAscope™ Hydrogen Peroxide and Protease Reagents | Bio-Techne | Cat#: 322381 |
| RNAscope® Target Retrieval Reagents | Bio-Techne | Cat#: 322000 |
| RNAscope® Wash Buffer Reagents | Bio-Techne | Cat#: 310091 |
| NF-Light V2 Advantage | Quanterix | Cat#: 104073 |
| MSD GOLD 96-well Small Spot Streptavidin Plates | Mesoscale Discovery | Cat#: L45SA-1 |
| V-PLEX Human Eotaxin-3 Kit | Mesoscale Discovery | Cat#: K151NUD |
| MSD GOLD SULFO-TAG NHS-Ester | Mesoscale Discovery | Cat#: R91AO-1 |
| NULISAseq™ CNS Disease Panel 120+ | Alamar Bioscience | N/A |
| NULISAseq™ Inflammation Panel 250 | Alamar Bioscience | N/A |
| Quick-RNA Miniprep Plus kit | Zymo Research | Cat#: R1058 |
| High-Capacity cDNA Reverse Transcription Kit | Thermo Fisher Scientific | Cat#: 4368814 |
| Pierce BCA Protein Assay | Thermo Fisher Scientific | Cat#: 23225 |
| EZ-Link™ Sulfo-NHS-LC-Biotin | Thermo Fisher Scientific | Cat#: A39257 |
| Octet® High Precision Streptavidin (SAX) Biosensors | Sartorius | Cat#: 18-5117 |
| RNaseAlert Substrate – 2 bulk tubes | IDT | Cat#: 11-04-02-03 |
| **Deposited data** | | |
| Raw proteomic data | This paper | ProteomeXchange, PrideID: PXD055796 |
| **Experimental models: Cell lines** | | |
| Expi293F | Thermo Fisher Scientific | A14527 |
| **Oligonucleotides** | | |
| Total *C9orf72* Taqman | Thermo Fisher Scientific | Cat #: 4351370; Assay ID: Hs00376619 |
| *C9orf72* Variant 1 Taqman | Thermo Fisher Scientific | Cat #: 4351370; Assay ID: Hs00331877 |
| *C9orf72* Variant 3 Taqman | Thermo Fisher Scientific | Cat #: 4351370; Assay ID: Hs00948764 |
| Truncated STMN2 (tSTMN2) Taqman | Thermo Fisher Scientific | Cat #: 4331348; Assay ID: APZTKFJ |
| *RPLP0* Endogenous Control Taqman (VIC™/MGB probe; primer limited) | Thermo Fisher Scientific | Cat#: 4326314E |
| *GAPDH* Endogenous Control (VIC™/MGB probe, primer limited) | Thermo Fisher Scientific | Cat#: 4326317E |
| C9ASO_5'Bio (/5BiotinTEG/GAGTCG+CGC) | IDT | N/A |
| C9ASO_3'DIG (GCTA+GGGGC/3Dig_N/) | IDT | N/A |
| BIIB078 (Tadnersen) Antisense Oligonucleotide | MedChemExpress | Cat#: HY-132581 |
| BIIB078 "ASO" (/52MOErG/*/i2MOErC// i2MOErC//i2MOErC/*/iMe-dC/*T* A*G*/ iMe-dC/*G*/iMe-dC/*G*/i2MOErC// i2MOErG//i2MOErA//i2MOErC/*/ i2MOErT/*/32MOErC/) | IDT | N/A |
| BIIB078 ASO 5' Biotin Modification (/5BiotinTEG//52MOErG/*/i2MOErC// i2MOErC/ /i2MOErC/*/iMe-dC/*T* A*G* / iMe-dC/*G*/iMe-dC/*G*/i2MOErC//i2MOErG// i2MOErA//i2MOErC/*/i2MOErT/*/32MOErC/) | IDT | N/A |
| BIIB078 "RNA" (rG*rCrCrC*rC*rU*rA* rG*rC*rG*rC*rG*rCrGrArC*rU*rC) | IDT | N/A |
| BIIB078 "DNA" (G*CCC*C*T*A*G* C*G*C*G*CGAC*T*C) | IDT | N/A |
| BIIB078 "mU" RNA (rG*rCrCrC*rC*/irT/*rA* rG*rC*rG*rC*rG*rCrGrArC*/irT/*rC) | IDT | N/A |

(*Continued on next page*)

Please cite this article in press as: McEachin et al., Molecular impact of antisense oligonucleotide therapy in *C9orf72*-associated ALS, Cell (2025), https://doi.org/10.1016/j.cell.2025.07.045



*Continued*

| REAGENT or RESOURCE | SOURCE | IDENTIFIER |
|---|---|---|
| BIIB078 "R/Dmid" (rG*rCrCrC*/iMe-dC/*T*A* G*/iMe-dC/*G*/iMe-dC/*G*rCrGrArC*rU*rC) | IDT | N/A |
| BIIB078 "MOE" (/52MOErG/*/i2MOErC// i2MOErC//i2MOErC/*/i2MOErC/*/i2MOErT/*/ i2MOErA/*/i2MOErG/*/i2MOErC/*/i2MOErG/*/ i2MOErC/*/i2MOErG/*/i2MOErC//i2MOErG// i2MOErA//i2MOErC/*/i2MOErT/*/32MOErC/) | IDT | N/A |
| ssRNA40 (rG*rC*rC*rC*rG*rU*rC*rU* rG*rU*rU*rG*rU*rG*rU*rG*rA*rC*rU*rC) | IDT | N/A |
| ssRNA40-Fluoro (/5Alex488N/rG*rC* rC*rC*rG*rU*rC*rU*rG*rU*rU*rG*rU*rG*rU*rG*rA*rC*rU*rC) | IDT | N/A |
| **Recombinant DNA** | | |
| Twin-StrepTag-RNASET2-WT | This Study | N/A |
| Twin-StrepTag-RNASET2-H65/118F | This Study | N/A |
| **Software and algorithms** | | |
| Methodical Mind | Mesoscale Discovery | N/A |
| R | The Comprehensive R Archive Network | https://cran.r-project.org/ |
| Fragpipe v19.0 | N/A | N/A |
| MSFragger v3.5 | N/A | N/A |
| Octet N1 | Sartorius | https://www.sartorius.com/ |
| **Other** | | |
| MSD Quickplex SQ120 | Mesoscale Discovery | N/A |
| Alamar ARGO System | Alamar Bioscience | N/A |
| Quantstudio 6 Flex System | Thermo Fisher Scientific | N/A |
| Orbitrap Astral Spectrometer | Thermo Fisher Scientific | N/A |
| Vanquish Neo | Thermo Fisher Scientific | N/A |

## METHOD DETAILS

### Lysate preparation

For protein immunoassays and proteomics, ~50 mg tissue was homogenized in 8M Urea buffer (8M Urea, 30 mM Tris pH8.0, 1x HALT protease/phosphatase inhibitor) at a 1:5 weight to volume ratio. Lysates were sonicated at 30% amplitude for 4 cycles of 2 seconds on/2 seconds off. Bicinchoninic acid (BCA) assay was used to determine protein lysate concentration. For POE immunoassays, ~50mg tissue was homogenized in POE lysis buffer (1% NP-40, 1x PBS) at 1:10 weight to volume ratio.

### miRNAscope in situ hybridization (ISH) Assay

miRNAScope assay was performed using ACDbio's protocol with additional modifications. In short, paraffin-embedded sections (8 μm) were deparaffinized in Histo-clear (National Diagnostics), incubated in 100% ethanol, dried out for 5 min at 60°C, and incubated in 10% neutral buffered formalin (NBF) overnight at room temperature (R.T.). Slides were subsequently washed for 2 min in dH2O and dried for 5 min at 60°C. Sections were treated with hydrogen peroxide for 10 minutes at R.T. to quench endogenous peroxidase activity and subsequently washed twice in dH2O. Slides were initially acclimated in dH2O for 10 sec in a steamer followed by antigen retrieval in 1x RNAscope® Target Retrieval buffer for 15 min. Tissue sections were treated with Protease III for 30 min at 40°C, rinsed twice in dH2O, and incubated with a custom miRNAscope probe for 2h at 40°C. The custom miRNAscopeTM probe was devised to specifically target antisense oligonucleotides (ASOs) against C9orf72 (Probe ID: SR-ASO-Hs-C9orf72-S1). miRNAscopeTM HD (RED) Assay kit was used to perform ISH signal amplification. All ISH AMP steps were followed by two washes in 1xRNAscope®. Slides were developed with miRNAscopeTM Fast Red substrate. Sections were subsequently counterstained with Gill's hematoxylin, blued in Scott's tap water substitute, and dried for 15 min at 60°C.

### CSF Neurofilament (NfL) Immunoassay

All CSF samples were assayed on the same instrument and by the same person in a blinded fashion. NfL concentrations in CSF were measured with the NF-Light V2 Advantage digital immunoassay (Quanterix, Cat#104073, Lot 503892) using the HD-X Analyzer per

Please cite this article in press as: McEachin et al., Molecular impact of antisense oligonucleotide therapy in *C9orf72*-associated ALS, Cell (2025), https://doi.org/10.1016/j.cell.2025.07.045



the manufacturer's protocol. In brief, samples were thawed on ice and diluted at 1:25 before transferring samples to 96-well plates. Samples were further diluted 1:4 by the instrument and tested in duplicate. In addition to participant CSF samples, the run included 8 calibrators, and 2 quality control samples provided with the kits that were tested in triplicate. Concentrations were interpolated from the standard curve using a 4-parameter logistic curve fit (1/y2 weighted).

### Meso-Scale Discovery (MSD) immunoassay (pTDP-43, polyGP, polyGA)

Phosphorylated TDP-43 measurements were performed using a custom MSD immunoassay. The capture antibody was a mouse monoclonal antibody that detects TDP-43 phosphorylated at serines 409/410 (1 μg/mL CAC-TIP-PTD-M01, Cosmo Bio USA), and the detection antibody was a sulfo-tagged rabbit polyclonal C-terminal TDP-43 antibody (1 μg/mL, 12892-1-AP, Proteintech). For poly(GP) immunoassays, an affinity purified monoclonal poly-GP antibody (TALS 828.179) generated by Target ALS was used as both the capture antibody (biotinylated TALS 828.179, 1 μg/mL), and the detection antibody (sulfo-tagged TALS 828.179, 1 μg/mL). Similarly, for poly(GA) MSD immunoassay, an affinity purified monoclonal poly-GA antibody (clone 5E9, Cat. #MABN889, Millipore Sigma) was used as both the capture antibody (5E9, 1 μg/mL), and the detection antibody (sulfo-tagged 5E9, 1 μg/mL). Lysates were diluted in 8M urea such that all samples of a given type were made up to the same concentration and an equal amount of protein for samples was tested in duplicate wells. Response values corresponding to the intensity of emitted light upon electrochemical stimulation of the assay plate using the MSD QUICKPLEX SQ120 were acquired. These response values were background corrected by subtracting the average response values from corresponding control lysates. Recorded values from MSD immunoassays are presented in arbitrary units.

### NULISAseq Assay

NULISAseq was performed at Alamar Bioscience as described in Feng et al.[34] In brief, 10μL of CSF of each sample was loaded into a 96 well plate and assayed for the either the NULISAseq CNS Panel 124 or NULISAseq Inflammation Panel 250. There are 52 overlapping targets between the CNS and Inflammation panel. The CNS panel is comprised of antibody pairs that target proteins associated with neurodegeneration and the Inflammation panel is comprised of antibody pairs that target inflammation and immune response related cytokines/chemokines. Immunocomplex formation with paired sets of oligo-conjugated antibodies, oligo-dT capture, strepavidine capture, and ligation were performed on the automated Alamar ARGO™ system. The DNA reporter library of target-specific molecular identifiers (TMI) and sample-specific molecular identifier (SMI) were pooled, PCR amplified and sequenced on an Illumina NextSeq 2000 system.

To identify proteins exhibiting sustained changes following BIIB078 administration, a moving average of NPQ values was calculated for each subject using a window size of three. Fold change was then determined by comparing the group mean of NPQ values at the final dose to the group mean at the first dose across all six subjects. Paired sample t-tests were performed for each target to calculate p-values, comparing NPQ values from the first and last doses. A volcano plot was then generated, with fold change on the x-axis and –log(p-value) on the y-axis.

### Immunohistochemistry

Paraffin embedded sections (8μm) were deparaffinized in Histo-clear (National Diagnostics) and rehydrated in ethanol. Antigen retrieval was performed in ddH2O by steam heat for 30 minutes. Endogenous peroxidase activity was quenched using hydrogen peroxide and washed 3 times in 0.05% PBS-Tween (PBS-T). Tissue sections were blocked using serum-free protein block (Dako) for 20 minutes. Slides were incubated in primary antibodies for 45 minutes at R.T. followed by 3 washes in PBS-T. Polymer HRP-conjugated secondaries (Dako) were applied for 30 minutes at R.T. Peroxidase labeling was visualized with 3,3'-diaminobenzidine (DAB). Sections were subsequently counterstained with Gill's hematoxylin and blued in Scott's tap water substitute.

For dual IHC, antigen retrieval was performed in ddH2O by steam heat for 30 minutes. Endogenous peroxidase activity was quenched using hydrogen peroxide for 5 minutes and washed 3 times in 0.05% PBS-Tween (PBS-T). Tissue sections were blocked using serum-free protein block (Dako) for 20 minutes. Slides were incubated in with anti-ASO primary antibody (1:5,000) for 45 minutes at R.T. followed by 3 washes in PBS-T. A polymer HRP-conjugated secondary (Dako) was applied for 30 minutes at R.T. followed by 3 washes in PBS-T. Peroxidase labeling was visualized with HRP Magenta Chromogen (Dako). Slides were wash 3 times in PBS-T. Slides were incubated in 0.3M sulfuric acid for 3 minutes to remove antibodies, followed by 3 washes with PBS-T. An additional peroxidase quenching step was performed using hydrogen peroxide for 5 minutes followed by PBS-T washes. Slides were incubated in anti-polyGA (1:3,000; clone 5E9, Cat. #MABN889, Millipore Sigma) second primary antibodies for 45 minutes at R.T. followed by 3 washes in PBS-T. A polymer HRP-conjugated secondary (Dako) was applied for 30 minutes at R.T. followed by 3 washes in PBS-T. Peroxidase labeling of the second antibody stain visualized with impact SG Substrate (Vector Laboratories). Sections were subsequently counterstained with Methyl Green.

### Plate-based oligonucleotide electro-chemiluminescent (POE) immunoassay

POE assay for ASO detection performed based on Neumann et al.[35] In short, 25 nM each of capture (C9ASO_5'Bio: /5BiotinTEG/GAGTCG+CGC) and detection (C9ASO_3'DIG: GCTA+GGGGC/3Dig_N/) oligonucleotides (IDT) were prepared in a volume of 50 μL with 1X TE buffer for duplicate reactions in the presence of BIIB078 ASO (Cat# HY-132581, MedChemExpress) for standards, or sample lysates. Sample lysates were homogenized in Addition of 50 μL of 2x SSC (saline sodium citrate) hybridization buffer

with 100μg/ml final Proteinase K (Thermo Fisher, EO0491). Hybridization reaction in PCR machine as follows: 50°C for 15 minutes, 95°C for 5 minutes, 40°C for 30 minutes, and 12°C for hold. Hybridized reactions were plated in duplicate onto MSD GOLD 96-well Small Spot Streptavidin plates (MSD, L45SA-1); incubated for 30 minutes at RT with shaking at 600rpm. Wells were washed 3 times with 1x PBS-T (0.05% Tween-20). Detection antibody (Sulfo-tagged Anti-Digoxigen, Novus Biologicals, NB100-65495) was added to wells at 0.5 ug/ml final in Superblock (Thermo Scientific, 37580) and incubated as before. Wells were washed 3 times with 1X PBS-T (0.05% Tween-20) then read in 150 μL of 1x MSD Read Buffer T by MSD QUICKPLEX SQ120. Standards were serially diluted 4-fold from 160 nM to 0.039 nM, with an additional blank well included. Standard curves were fitted using a four-parameter logistic model in MSD Discovery Workbench software to determine the concentrations of unknown samples. Concentrations were back-calculated to reflect a 1x tissue-equivalent concentration, accounting for dilution during tissue homogenization in lysis buffer.

### RNA extraction and quantitative reverse transcription with PCR (RT-PCR)

RNA was extracted using the Quick RNA kit (Zymo Research) with a combined on-column DNase I digestion step. For RNA extraction from post-mortem tissue, ∼30 mg of tissue was homogenized in lysis buffer using a bullet blender tissue homogenizer (Next Advance). RNA lysates were cleared by spinning samples at 10,000g for 1 minute. RNA extraction was performed as per the manufacture's protocol, concentration was measured with a Synergy

H1 Multi-Mode Plate Reader, and RNA integrity assess with a Bioanalyzer. Only spinal cord tissue RNA with RIN values >5 were used for downstream qPCR applications. cDNA was obtained via RT-PCR using the High-Capacity cDNA Reverse Transcription Kit (Thermo). 1000 ng total RNA was used for cDNA reactions; cDNA was diluted 1:2 with nuclease free water. To quantify relative mRNA expression of *C9orf72* and t*STMN2*, qPCR was performed for each sample using predesigned and custom Taqman gene expression assays (Thermo) on a Quantstudio 6 Flex system (Applied Biosystems). For each sample, 4 μL of cDNA, corresponding to ∼67 ng of input RNA, were loaded per well in duplicate for qPCR. The Ct method was used to assess relative expression. Relative tissue RNA expression was normalized to RPLP0 and GAPDH; specifically, the geometric mean of RPLP0 and GAPDH Ct values was calculated and subtracted from the Ct value for each cryptic exon Taqman tested to generate a sample specific ΔCt. The ΔCt values for the healthy control samples were averaged to generate an averaged control group ΔCt value (ΔCtAVG). ΔΔCt values were calculated by subtracting the ΔCtAVG from the ΔCt of each sample. Relative expression was calculated using $2^{(-\Delta\Delta Ct)}$.

### Neonatal Intracerebroventricular (ICV) Injections

Intracerebroventricular injections of BIIB078 ASO (Cat# HY-132581, MedChemExpress) were carried out in neonatal B6 wild-type mice as follows. Two microliters of ASO were administrated bilaterally into the cerebral ventricle. PBS injections served as control. At weaning pups were euthanized, brains were harvested and one hemibrain was fixed overnight in 4% paraformaldehyde at 4°C followed by processing and paraffin embedding for immunohistochemical staining. The other hemibrain was snap-frozen in isopentane on dry ice and then stored at -80°C for further analysis.

### Production and purification of recombinant RNase T2 protein

A codon optimized DNA sequence encoding amino acids 1-24 (signal peptide) of RNase T2, Twin-StrepTag, and amino acids 25-256 of RNase T2 was synthesized as a gBlock (Integrated DNA Technologies). A second gBlock was synthesized with the same sequence but with mutations converting the conserved histidine residues to phenylalanine in the two respective conserved active site (CAS) domains (H65/118F), resulting in a catalytically inactive protein. Synthesized gBlocks were cloned into pcDNA3.1 using NheI and BamHI.

The protein expression plasmids were individually transfected into Expi293F cells (Thermo Fisher Scientific) using the ExpiFectamine™ 293 Transfection Kit following the manufacturer's instructions. For each plasmid, cells were seeded at a density of $3 \times 10^6$ cells in 60 mL of Expi293 medium and maintained at 37 °C with 8% $CO_2$ under shaking conditions (125 rpm).

For transfection, 60 μg of plasmid DNA was diluted in 3 mL of Opti-MEM™ I serum-free medium and filtered. Separately, 180 μL of ExpiFectamine™ 293 reagent was mixed with 3 mL of Opti-MEM™, gently swirled, and incubated for 5 minutes. The solutions were then combined, incubated for 20 minutes, and added to the cell culture.

After 20 hours of incubation under shaking conditions, 300 μL of Transfection Enhancer-1 and 3 mL of Transfection Enhancer-2 were added. Cells were cultured for six days post-transfection. The culture was then centrifuged at 4,000 × g for 20 minutes at 4 °C, and the supernatant was collected and filtered through a 0.45 μm membrane.

To block free biotin in the culture medium that could interfere with Strep-Tactin® XT purification, BioLock™ (IBA Lifesciences) was added according to the manufacturer's recommendations. A protease inhibitor cocktail (Sigma-Aldrich) was also added to prevent protein degradation.

The clarified supernatant was run through a 1 mL Strep-Tactin® XT 4Flow® column (IBA Lifesciences) pre-equilibrated with Buffer A (50 mM HEPES, 150 mM NaCl, pH 8.0) using the NGC chromatography system (Bio-Rad) at a flow rate of 0.5 mL/min. Unbound proteins were removed by washing with 10 mL of Buffer A. Bound proteins were eluted with 10 mL of Buffer A containing 50 mM D-(+)-biotin (Enzo). The first six column volumes (CVs) of elution fractions were pooled and dialyzed against 1x PBS and concentrated using the Amicon® Ultra-15 Centrifugal System (Millipore). Protease inhibitors were added, and the purified proteins were quantified using the BCA assay before storage at -80 °C.

Please cite this article in press as: McEachin et al., Molecular impact of antisense oligonucleotide therapy in *C9orf72*-associated ALS, Cell (2025), https://doi.org/10.1016/j.cell.2025.07.045



### RNase T2 Cleavage Assays

Oligonucleotides at a concentration of 1 μM were incubated with 50 nM of recombinant human RNase T2 in 1x cleavage (50 nM Sodium Acetate, 100 nM NaOH, pH4.5) for 15 min at 37°C in a 10 μL total reaction volume. An equal volume of TBE-urea sample buffer (2x) was added to each reaction and incubated at 95°C for 5 min. Samples were separated on a 15% TBE-urea gel for 45min at 250V. The gel was incubated with 1x SYBR gold diluted in 1x TBE for 10 min and then imaged on a BioRad ChemiDoc.

### Nuclease Competition Assay

For Urea-PAGE competition assays, 50 nM of recombinant human RNase T2 was incubated with increasing concentrations of BIIB078 (2-fold difference from 160 nM to 40 μM) in 1x cleavage buffer for 15 min at 37°C. One microliter of a 5 uM stock of a 5' FAM modified ssRNA40 (corresponding to a final concentration of 500 nM) was added to each tube and incubated for an additional 15 min at 37°C. The cleavage reaction was stopped by the addition of an equal volume of 2x TBE-Urea sample buffer (Thermo) followed by incubation at 95°C for 5 min.

For fluorophore-quenched nuclease competition assays, 5 nM of recombinant RNase T2 and increasing concentrations of BIIB078 (0 nM to 5 μM) were mixed in 1x cleavage buffer (5 0nM Sodium Acetate, 100 nM NaOH, pH4.5); a total reaction volume of 50 uL was added to a clear bottom, black 96 well in duplicate wells. A commercial fluorophore-quenched ribooligonucleotide (RNaseAlert Substrate; IDT) was immediately added. Fluorescence was measured (493nm excitation/520nm emission) on a BioTek synergy H1 instrument every 45 seconds for 1 hour. All time points were background subtracted from the initial reading for each well.

### Bio-layer interferometry (BLI) binding assays

Bio-layer interferometry experiments were conducted using a ForteBio Blitz system. A streptavidin high-precision SAX biosensor (Sartorius) was loaded and incubated in 1x binding buffer (50 mM sodium acetate, 100 mM NaOH, 0.02% Triton X-100, pH 4.5) for 30 seconds. The biosensor was then incubated with 4 μL of 1 μM biotin-labeled BIIB078 ASO for 120 seconds. After loading, the BIIB078-coated biosensor was incubated in 1x binding buffer for 30 seconds. Subsequently, the BIIB078-loaded biosensor was incubated in 4 μL of increasing concentrations of RNase T2 for 120 seconds ("association" phase), followed by incubation in 1x binding buffer for 120 seconds ("dissociation" phase). Working stocks of biotin-labeled BIIB078 and recombinant RNase T2 were prepared by dilution in 1x binding buffer. A 1:1 binding model using a global fit method was used to calculate kinetic parameters (Sartorius Octet N1 Software)

### Tissue Homogenization and Protein Digestion

Samples (100 μg) were reduced with 5 mM IAA and 10mM DTT at room temperature (each for 30 mins) in the dark. Samples were diluted to 4M Urea and digestion was started with the addition of 5 ug of Lysyl endopeptidase (Wako) and allowed to proceed overnight. Samples were then 4-fold diluted with 100mM Tris and 5 μg of trypsin (ThermoFisher Scientific) and digestion proceeded overnight. The peptide solutions were acidified to a final concentration of 1% (vol/vol) formic acid (FA) and 0.1% (vol/vol) trifluoroacetic acid (TFA) and desalted with a 10 mg HLB column (Oasis). Each HLB column was first rinsed with 1 mL of methanol, washed with 1 mL 50% (vol/vol) acetonitrile (ACN), and equilibrated with 2×1 mL 0.1% (vol/vol) TFA. The samples were then loaded onto the column and washed with 2×1 mL 0.1% (vol/vol) TFA. Elution was performed with 2 volumes of 0.5 mL 50% (vol/vol) ACN. Samples were dried by SpeedVac (LabConco).

### Isobaric Tandem Mass Tag (TMT) Peptide Labeling

Each sample was re-suspended in 100 mM TEAB buffer (50 μL). The TMTpro labeling reagents (5 mg) were equilibrated to room temperature, and anhydrous ACN (200 μL) was added to each reagent channel. Each channel was gently vortexed for 5 min, and then 10 μL from each TMT channel was transferred to the peptide solutions and allowed to incubate for 1 h at room temperature. The reaction was quenched with 5% (vol/vol) hydroxylamine (5 μl) (Pierce). All channels were then combined and dried by SpeedVac (LabConco). The combined sample was then resuspended in 500 uL of 0.1% TFA and then diluted 1:1 with 4% H3PO4 and desalted with a 30 mg MCX column (Waters). Samples were loaded onto the MCX column and then washed with 100 mM ammonium formate in 2% formic acid. This is followed by a methanol wash and finally the samples were eluted with 300 μL of 5% ammonium hydroxide in methanol. The eluates were then dried to completeness using a SpeedVac (LabConco).

### High-pH Off-line Fractionation

Dried samples were re-suspended in high pH loading buffer (0.07% vol/vol NH4OH, 0.045% vol/vol FA, 2% vol/vol ACN) and loaded onto a Water's BEH 1.7 um 2.1mm by 150mm. A Thermo Vanquish was used to carry out the fractionation. Solvent A consisted of 0.0175% (vol/vol) NH4OH, 0.01125% (vol/vol) FA, and 2% (vol/vol) ACN; solvent B consisted of 0.0175% (vol/vol) NH4OH, 0.01125% (vol/vol) FA, and 90% (vol/vol) ACN. The sample elution was performed over a 25 min gradient with a flow rate of 0.6 mL/min. A total of 192 individual equal volume fractions were collected across the gradient and subsequently pooled by concatenation into 96 fractions and dried to completeness using a SpeedVac.

Please cite this article in press as: McEachin et al., Molecular impact of antisense oligonucleotide therapy in *C9orf72*-associated ALS, Cell (2025), https://doi.org/10.1016/j.cell.2025.07.045



### Liquid Chromatography Tandem Mass Spectrometry

All fractions were resuspended in an equal volume of loading buffer (0.1% FA, 0.03% TFA, 1% ACN) and analyzed by liquid chromatography coupled to tandem mass spectrometry. Peptide eluents were separated on Water's CSH column (1.7um resin 150um by 15 cm) by a Vanquish Neo (ThermoFisher Scientific). Buffer A was water with 0.1% (vol/vol) formic acid, and buffer B was 99.9% (vol/vol) acetonitrile in water with 0.1% (vol/vol) formic acid. The gradient was from 3% to 35% solvent B over 17 mins followed by column wash and equilibration for a total of 23 mins. Peptides were monitored on a Orbitrap Astral mass spectrometer (ThermoFisher Scientific) fitted with a high-field asymmetric waveform ion mobility spectrometry (FAIMS Pro) ion mobility source (ThermoFisher Scientific). Two compensation voltages (CV) of -45 and -60 were chosen for the FAIMS. Each cycle consisted of one full scan acquisition (MS1) with an m/z range of 400-1500 at 120,000 resolution and standard settings and as many tandem (MS/MS) scans in 1.5 seconds. The Astral higher energy collision-induced dissociation (HCD) tandem scans were collected at 35% collision energy with an isolation of 0.5 m/z, an AGC setting of 100%, and a maximum injection time of 20ms. Dynamic exclusion was set to exclude previously sequenced peaks for 30 seconds within a 5-ppm tolerance window.

### Database Searches and Protein Quantification

All raw files underwent a database search using Fragpipe (version 19.0). The database search parameters have been described.[56] Initially, mzML files were created from the original MS.raw files for spinal cord using the ProteoWizard MSConvert tool (version 3.0) with specific options, including 'Write index,' 'TPP compatibility,' 'Use zlib compression,' and a "peakPicking" filter setting.

Following the creation of mzML files for each set, they were subjected to a search using MSFragger (version 3.5). The human proteome database used contained 20,402 sequences (Swiss-Prot, downloaded 2/11/2019) along with corresponding decoys and common contaminants.

The search settings included a precursor mass tolerance of -20 to 20 ppm, a fragment mass tolerance of 20 ppm, mass calibration, parameter optimization, isotope error set to -1/0/1/2/3, strict-trypsin enzyme specificity, and allowance for up to two missed cleavages. Fully enzymatic cleavage type, peptide length (7 to 50), and peptide mass (200 to 5,000 Da) criteria were defined. Variable modifications included oxidation on methionine, N-terminal acetylation on protein, and TMTpro modification on the peptide N-terminus, with a maximum of 3 variable modifications per peptide. Static modifications comprised isobaric TMTpro (TMT16) modifications on lysine, along with carbamidomethylation of cysteine.

Post-MSFragger (version 3.6) search, Percolator[57] was used for PSM validation, succeeded by Philosopher (version 4.6.0) for protein inference using ProteinProphet and FDR filtering. Reports containing quantified peptides and UniprotID-identified proteins with an FDR < 1% were generated. The database search culminated in the identification of a total of 9,694 protein groups. Before performing any abundance analysis, the data from all batches were merged and protein levels were first scaled by dividing each protein intensity by intensity sum of all proteins in each sample followed by multiplying by the maximum protein intensity sum across all samples. Instances where the intensity was '0' were treated as 'missing values'.

### Bioinformatics processing and statistical analysis

To account for batch variation, we employed a Tunable Approach for Median Polish of Ratio (TAMPOR)[58] along with removal of peptides or proteins absent in 50% or more of cases, as previously published.[38,59] To ensure data reliability, we identified and removed outliers that were >3 SD below the mean sample connectivity as determined by WGCNA as determined by the fundamentalNetworkConcepts function run on a bicor adjacency matrix. We next performed parallelized, ordinary, nonparametric, bootstrapping regression to remove age, sex, brain bank, TMT batch, and residual batch effects using an established pipeline.[38,59] One-way ANOVA with Tukey's HSD (Honestly Significant Difference) correction was performed using an in-house script (https://github.com/edammer/parANOVA) to identify peptides and proteins that were differentially expressed. Additionally, multiple testing correction was performed within each disease groups using Benjamini-Hochberg correction or permutation based false discovery rate (FDR) correction via the ROTS package[60] (Table S2). Differential abundance is presented as volcano plots, displaying $\log_2$ fold change versus the negative $\log_{10}$ of the Tukey's HSD corrected p-value.

## QUANTIFICATION AND STATISTICAL ANALYSIS

All data are displayed as box plots displaying the median and interquartile range (IQR). Statistical analysis of qPCR data was performed on ΔCt values. Statistical analysis of qPCR was performed using the Kruskal-Wallis test. Pairwise comparisons across all groups were performed with Conover-Iman's post hoc analysis with Bonferroni correction for multiple comparisons. MSD immunoassay data was performed using the Mann Whitney test. Only drug-naïve and BIIB078-treated c9ALS cases were considered for analysis. All samples were included in MSD statistical analyses. For visualization purposes, within group outliers as determined by Grubb's test, were not shown. Kendall's $\tau$ rank correlation coefficient was used to assess the correlation of BIIB078 ASO concentration and various dosing parameters. Pearson correlation coefficient was used to assess correlation between BIIB078 concentration and *C9orf72* transcript expression.

CellPress
OPEN ACCESS

# Supplemental figures

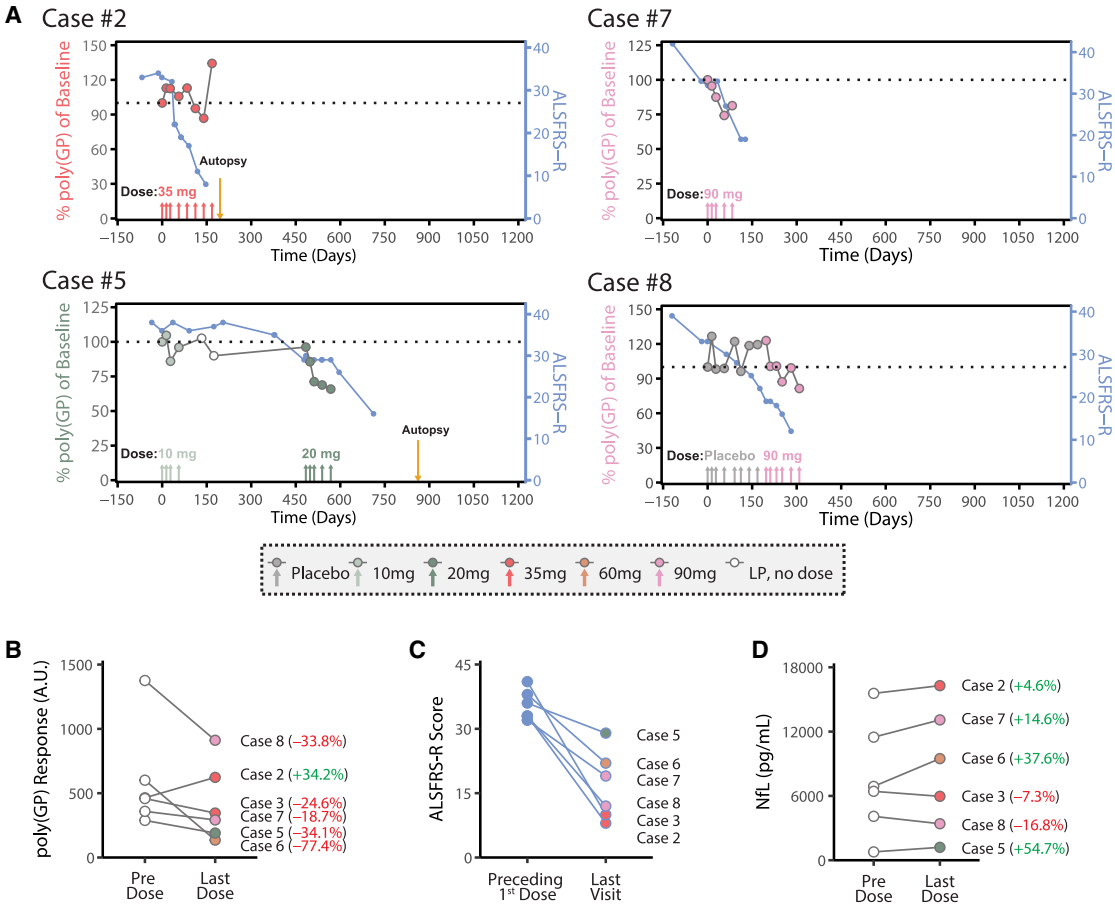


**Figure S1. Poly(GP) DPRs are reduced in the CSF of c9ALS patients treated with the sense strand-targeting ASO BIIB078, related to Figure 1**

(A) Timeline of BIIB078 dosing, CSF poly(GP) abundance, and ALSFRS-R scores. CSF was collected prior to dosing at each time point. Left axis shows relative CSF poly(GP) abundance normalized to a baseline (100%, dotted line); right axis shows ALSFRS-R scores recorded near-contemporaneously. Cases #3 and #6 are presented in Figure 1.

(B) Slope plot of raw poly(GP) abundance (A.U., arbitrary units) in CSF as measured by immunoassay at baseline and last dose for each case.

(C) Slope plot of ALSFRS-R measured at most proximal visit preceding first dose and last visit after terminal BIIB078 dose.

(D) Slope plot of neurofilament light-chain (NfL) abundance measured in CSF by immunoassay at visit preceding first BIIB078 dose and last dose for each case.

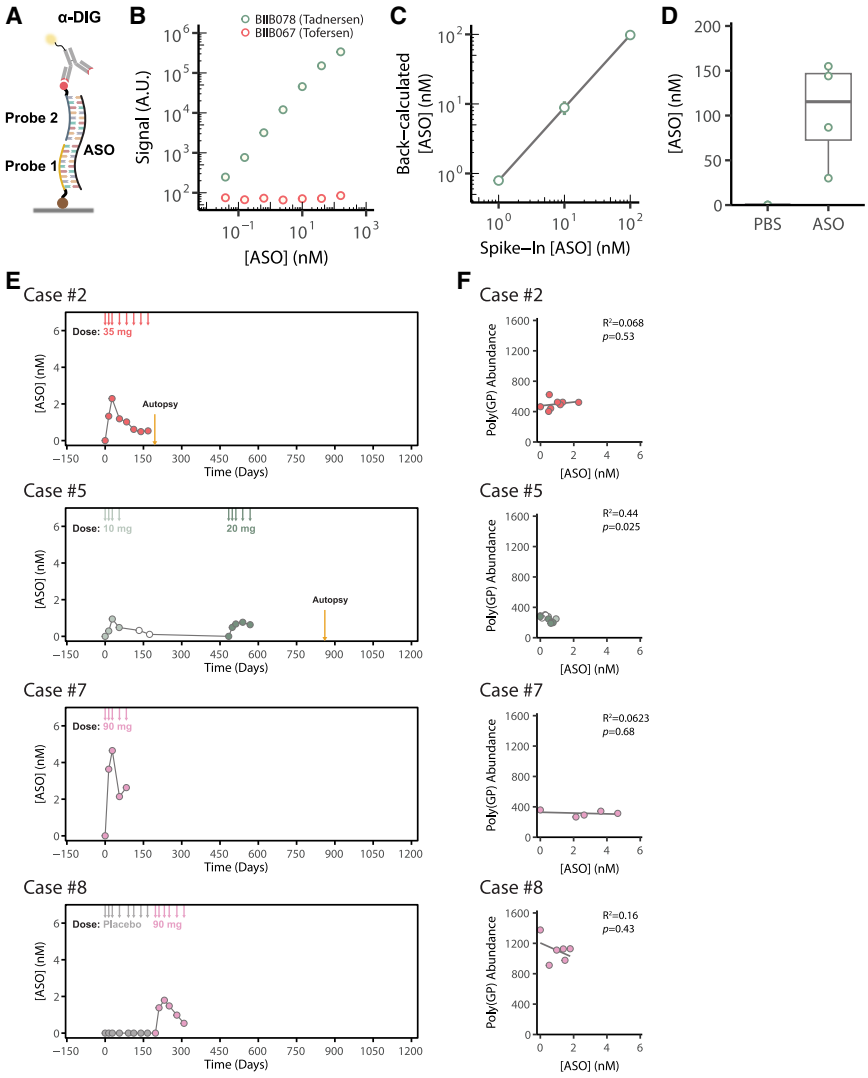


**Figure S2. Validation of BIIB078 POE assay and assessment of BIIB078 concentration in CSF, related to Figure 1**

(A) Schematic of plate-based oligonucleotide electrochemiluminescent (POE) assay.

(B) POE immunoassay specifically detects BIIB078 (tadnersen) but not another RNase-H competent ASO, BIIB067 (tofersen). 4-fold dilutions from 160 to 0.039 nM.

(C) BIIB078 POE assay accurately quantifies BIIB078 ASO spiked into human control lysate at various concentrations; *n* = 3 separate cases per concentration tested.

(D) BIIB078 POE assay specifically detects BIIB078 in mice injected with BIIB078 ASO but not in mice injected with PBS via ICV.

(E) Timeline and summary of BIIB078 dosing, CSF BIIB078 ASO concentration. CSF was collected prior to BIIB078 dosing at each time point.

(F) Correlation between BIIB078 ASO concentration and poly(GP) abundance for each time point. Pearson correlation.

For (E) and (F), cases #3 and #6 are presented in Figure 1.

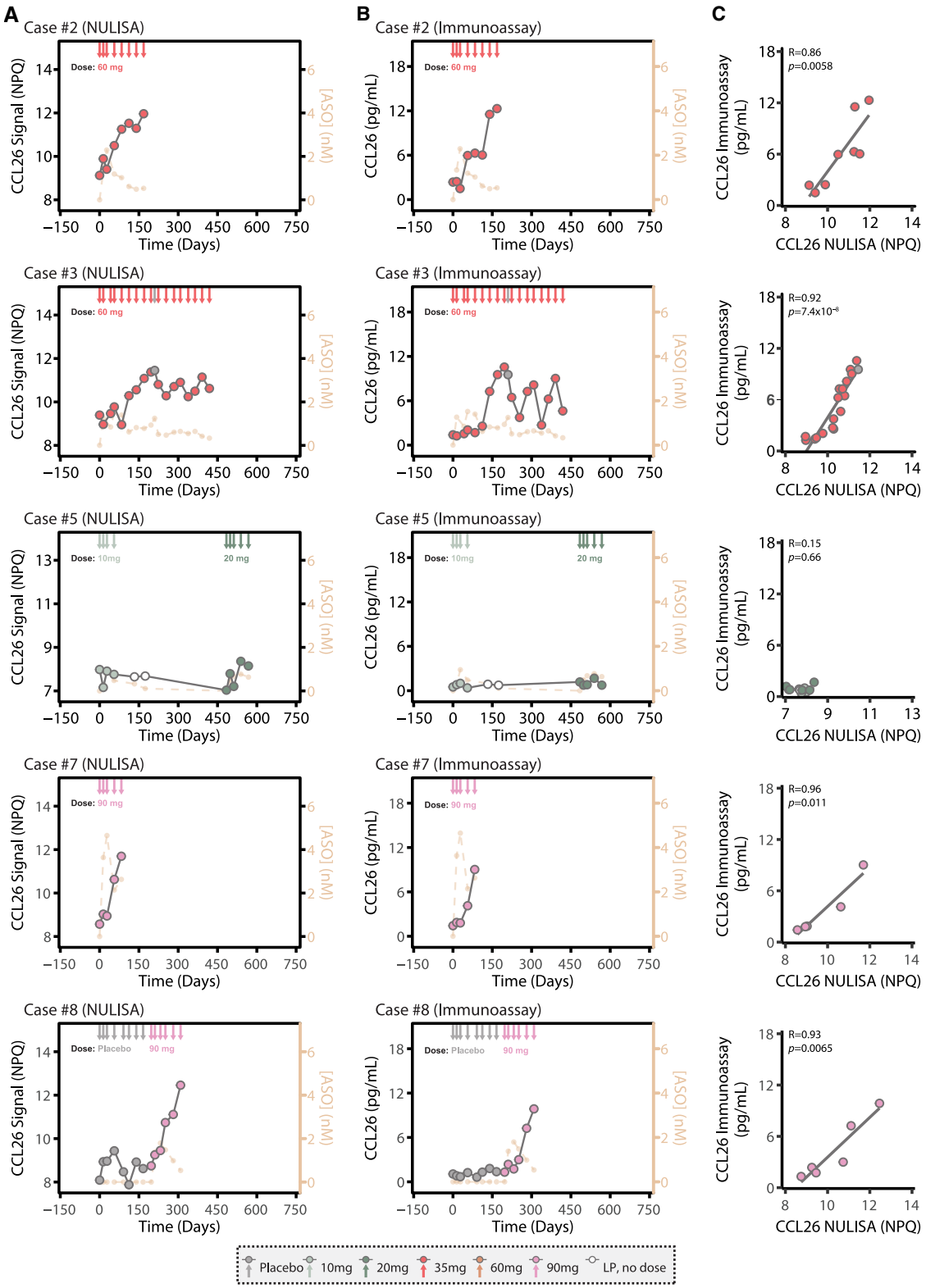


(legend on next page)

**Figure S3. Longitudinal assessment of CCL26 abundance in BIIB078-treated c9ALS cases, related to Figure 1**

(A and B) Measurement of CCL26 abundance by NULISA (A) and Mesoscale Discovery (MSD) immunoassay (B) for all BIIB078-treated c9ALS cases ($n$ = 6 cases; 79 total CSF time points).

(C) CCL26 abundance as measured by NULISA strongly correlates with abundance measured by MSD immunoassay. Pearson correlation. Case #6 is presented in Figure 1.

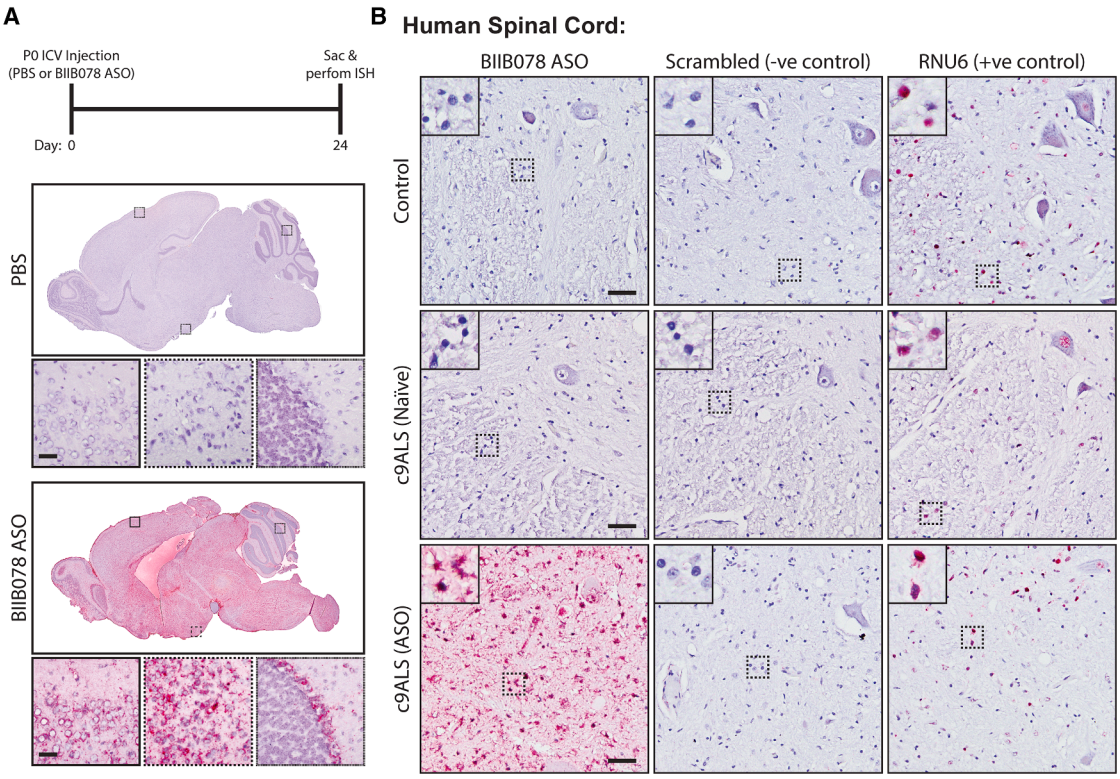


**Figure S4. Validation of custom miRNAscope probe targeting BIIB078 ASO, related to Figure 2**

(A) Top: schematic of mice injected with a single ICV bolus of PBS or BIIB078. Bottom: custom miRNAscope assay specifically detects BIIB078 ASO in mice injected with BIIB078 but not PBS. Scale bar, 30 μm.

(B) BIIB078 ASO is detectable by miRNAscope ISH in the spinal cord of a BIIB078-treated c9ALS case but not a non-ALS control or drug-naive c9ALS case; a scrambled and RNU6 probe included as negative and positive controls for ISH assay. Scale bar, 50 μm.

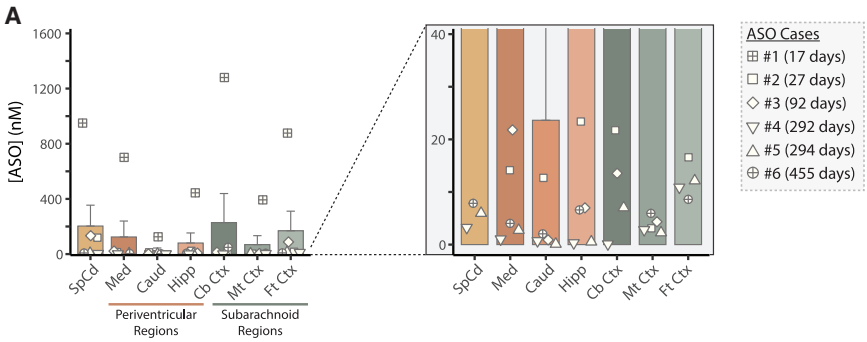


**Figure S5. BIIB078 POE assay across CNS regions, related to Figure 2**

BIIB078 concentrations in BIIB078-treated c9ALS cases across various CNS regions.

CellPress
OPEN ACCESS

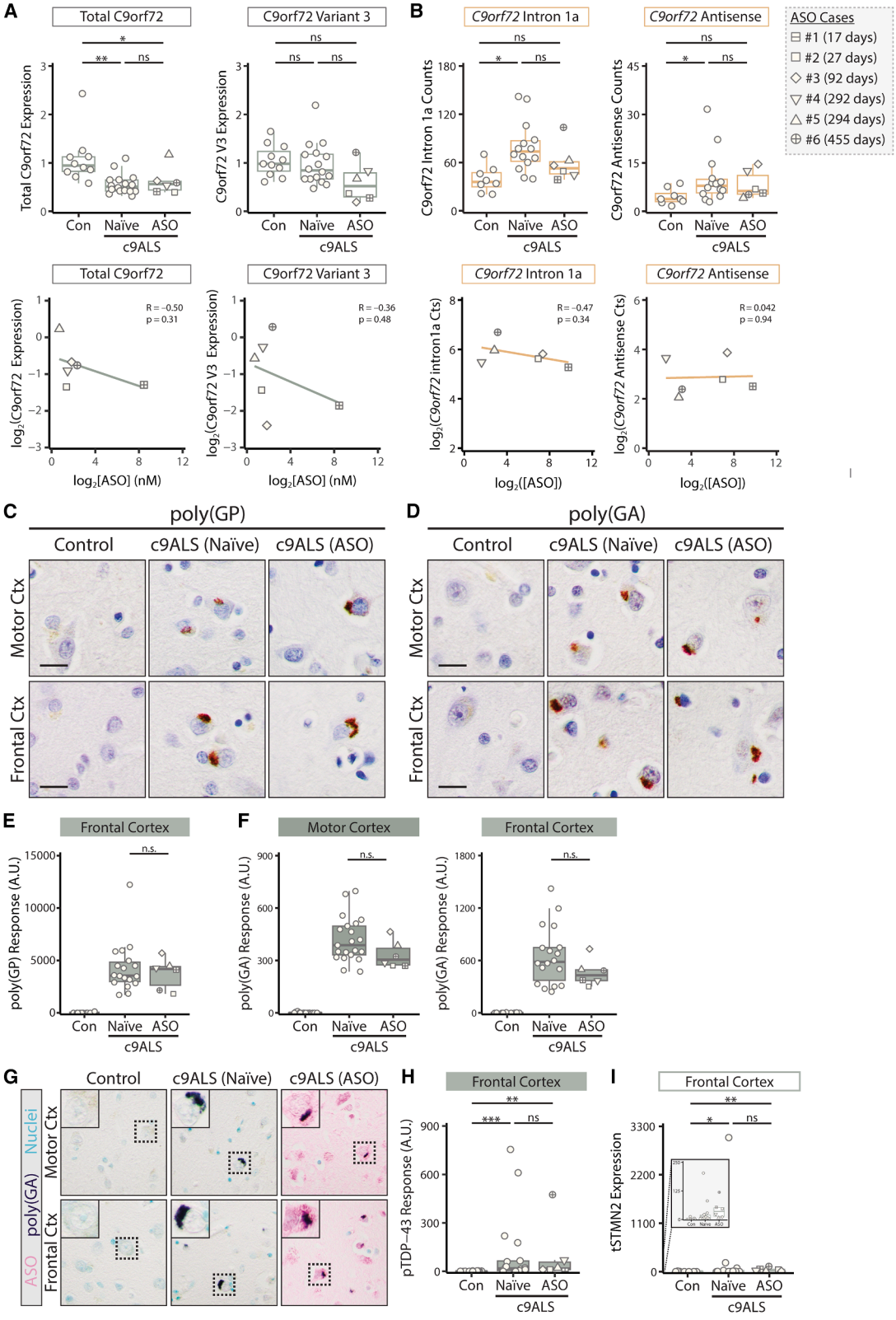


*(legend on next page)*

**Figure S6. Assessment of *C9orf72*-associated neuropathology in disease relevant brain regions in BIIB078-treated cases, related to Figure 3**

(A) Top: qPCR for total and variant 3 (V3) *C9orf72* expression in motor cortex. $n$ = 11 control, $n$ = 16 drug-naive c9ALS, $n$ = 6 BIIB078-treated c9ALS cases. Bottom: correlation of total and transcript-specific C9orf72 expression and BIIB078 ASO concentration. A moderate correlation between C9orf72 transcript V3 expression with BIIB078 ASO concentration was observed.

(B) Top: NanoString analysis for *C9orf72* intron containing transcripts, intron 1a, and antisense in spinal cord. Bottom: correlation of intron containing *C9orf72* transcripts and BIIB078 ASO concentration.

(C and D) Immunopositive poly(GA) and poly(GP) inclusions were detected in the motor cortex and frontal cortex of drug-naive (naive) and BIIB078-treated (ASO) cases. Scale bar, 30 μm.

(E) Quantification of poly(GP) abundance via MSD immunoassay in the frontal cortex shows abundant poly(GP) DPRs in drug-naive and BIIB078-treated c9ALS cases.

(F) Quantification of poly(GA) abundance via MSD immunoassay in the motor cortex and frontal cortex shows abundant poly(GA) DPRs in drug-naive and BIIB078-treated c9ALS cases.

(G) BIIB078 ASO and poly(GA) inclusions co-occur in the same cell as detected by double staining immunohistochemistry in BIIB078-treated cases.

(H) Quantification of pTDP-43 abundance via MSD immunoassay in the frontal cortex of control, drug-naive c9ALS, and BIIB078-treated cases.

(I) qPCR analysis of tSTMN2 expression in frontal cortex.

In (A), (B), (H), and (I), Kruskal-Wallis test followed by Conover-Iman post hoc comparisons with Bonferroni correction. In (E) and (F), only comparisons between drug-naive and BIIB078-treated c9ALS cases were considered. Mann-Whitney test. Motor cortex: $n$ = 17 control, $n$ = 21 drug-naive c9ALS, $n$ = 6 BIIB078-treated c9ALS cases. Frontal cortex: $n$ = 12 control, $n$ = 18 drug-naive c9ALS, $n$ = 6 BIIB078-treated c9ALS cases. $^{*}p < 0.05$, $^{**}p < 0.01$, $^{***}p < 0.001$, $^{****}p < 0.0001$.

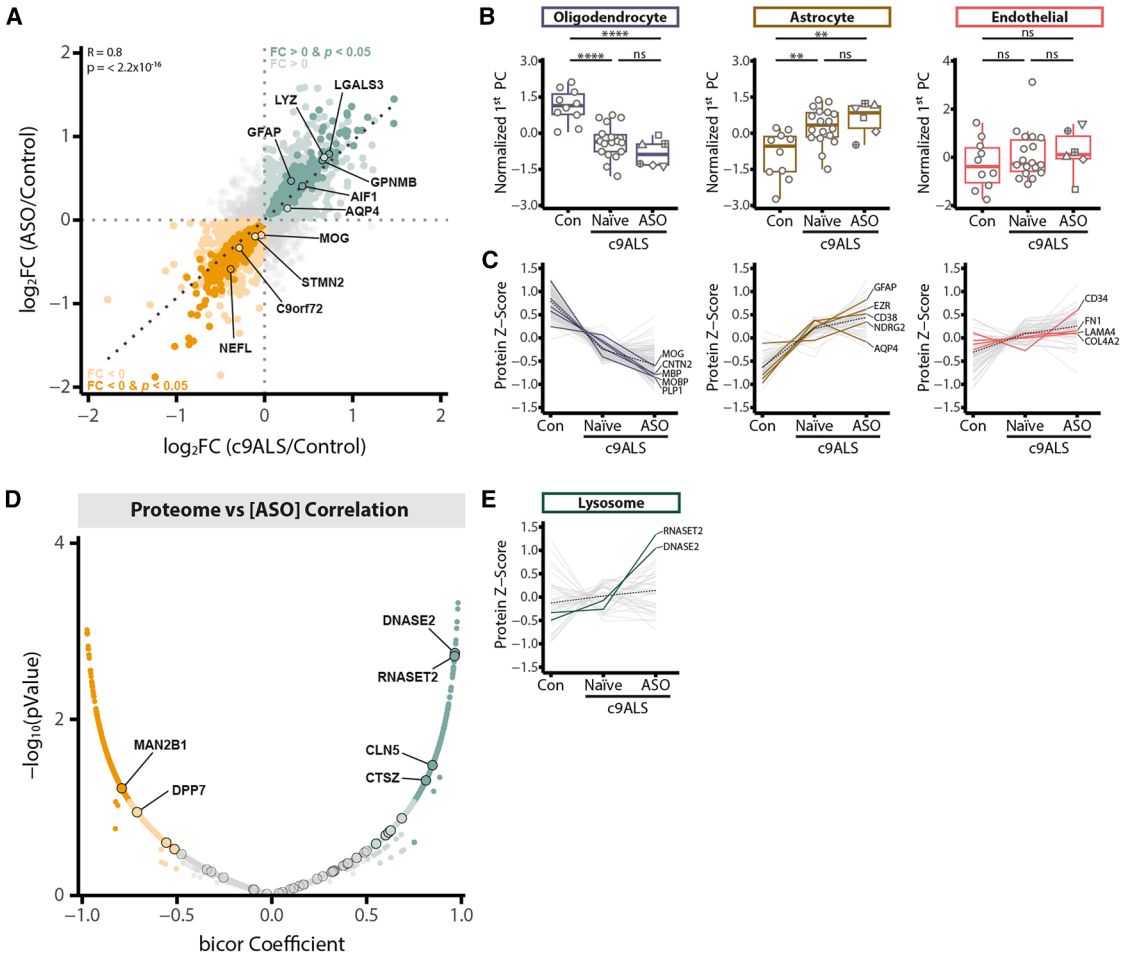


**Figure S7. Upregulation and correlation of RNase T2 and DNase II are independent of lysosomal protein abundance changes, related to Figure 4**

(A) Scatterplot of protein $\log_2$ fold changes between drug-naive c9ALS and control cases (*x* axis) and BIIB078-treated c9ALS and control cases (*y* axis).

(B) Boxplots of *Z* score-normalized eigenprotein values (first principal component) representing variance in curated cell-type marker proteins.

(C) Line plots of *Z* scored individual protein abundances from the respective cell-type marker list (Table S2); dotted black line represents mean *Z* scored value across proteins.

(D) Volcano plot displaying the biweight midcorrelation coefficient (*x* axis) against the −log10 statistical *p* value between all protein abundances and BIIB078 concentration in the spinal cord of BIIB078-treated c9ALS cases ($n = 6$ cases). Proteins from an established lysosomal protein list are highlighted by black circle outlines.

(E) Line plots showing the *Z* scored value for individual proteins from an established list of lysosomal proteins (Table S2). Dotted black line represents mean *Z* scored value for all proteins.

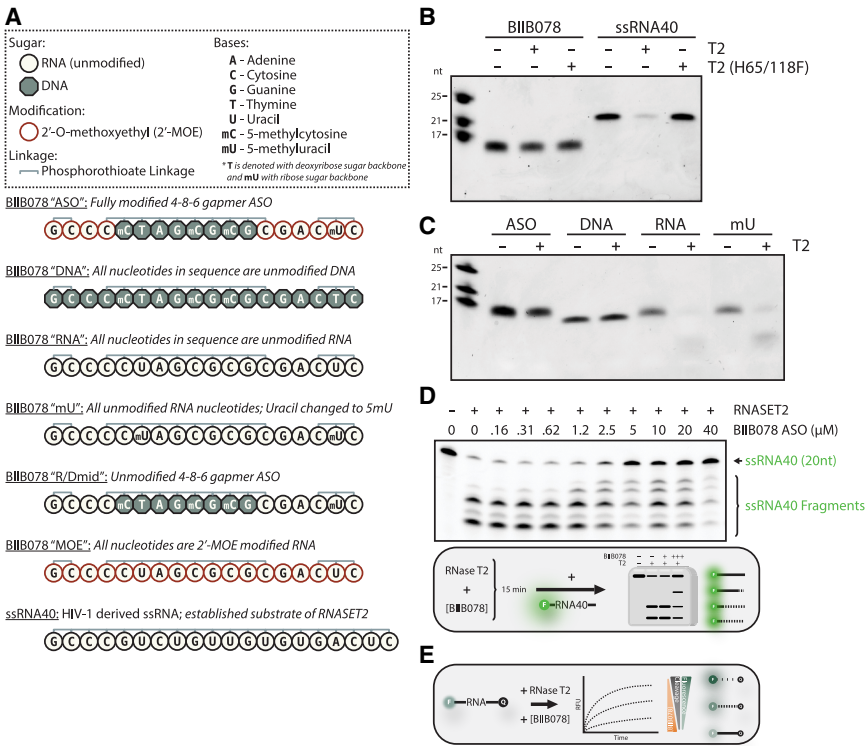


**Figure S8. BIIB078 is not cleaved but binds RNase T2 and modulates cleavage efficiency, related to Figure 4**

(A) Schematic depicting various BIIB078-derived oligo(ribo)nucleotides synthesized for cleavage assays.

(B) Urea-PAGE of BIIB078 or RNA40 digested with RNase T2 or a catalytically inactive RNase T2 (H65/118F).

(C) Urea-PAGE of BIIB078-derived oligo(ribo)nucleotides with RNase T2.

(D) Urea-PAGE of a fluorogenic RNA40 (1 μM) digested for 15 min with RNase T2 (50 nM) after a 15-min preincubation with various concentrations of BIIB078.

(E) Schematic of FAM-labeled fluorescence-quenched oligoribonucleotide assay presented in Figure 4. Uncropped gel images provided in Data S2.